Department of Chemistry – Radiochemistry

University of Helsinki

Finland

Ion Exchange in Nuclear Fuel Reprocessing – Zirconium Phosphate Materials for the Separation of Trivalent Actinides and Lanthanides

Elmo W. Wiikinkoski

ACADEMIC DISSERTATION

To be presented, with the permission of the Faculty of Science of the University of Helsinki, for public examination in lecture hall A110 in Chemicum, A.I. Virtasen aukio 1, on November 29th at 12 noon.

Helsinki 2019

Supervisors:

University Researcher, Docent Risto Koivula, Ph.D.

University of Helsinki

Professor Risto Harjula, Ph.D.

University of Helsinki

Pre-examiners:

Professor Ulla Lassi, D.Sc. (Tech.)

University of Oulu

Professor Tuomo Sainio, D.Sc. (Tech.)

LUT University of Technology

Dissertation opponent:

Associate Professor Eveliina Repo, D.Sc. (Tech.)

LUT University of Technology

ISSN 0358-7746

ISBN 978-951-51-5672-3 (paperback)

ISBN 978-951-51-5673-0 (electronic)

http://ethesis.helsinki.fi

Unigrafia

Helsinki 2019

Abstract

Each nuclear energy country has their strategy for handling the spent nuclear fuel: direct disposal, recycling or a combination of both. The advances in nuclear fuel partitioning enhance the safety of both of these approaches. The spent fuel contains fissionable material that could be used in modern and future reactors. The re-use, however, requires a separation of the fissionable material from the neutron poisoners that are also present in the spent fuel. Time-proven separation technologies exist for the recovery of uranium and plutonium, but for the trivalent actinides americium and curium, such technologies are still young.

The majority of current separation technologies in nuclear fuel partitioning, such as the solvent extraction, are based on the recovery of target nuclides from liquids by organic extractants. Their application can be limited by the high radiation doses during the separation process. Ion exchange with inorganic materials offers a robust supportive role in the separation challenges for radionuclides. The materials are stable in high temperatures, high acidity and under extreme radiation, and are ion selective. By altering their structure, the desired ion selectivity can be further improved.

Throughout the dissertation, a solid inorganic ion exchanger, α-zirconium phosphate, was investigated, developed and applied in column operation with one goal in mind: the application of ion exchange in the column separation of trivalent actinides from lanthanides.

The α-zirconium phosphate proved suitable for americium-europium separation. The material was modified and the connections between synthesis, properties and ion selectivity between various products were investigated and discussed. Numerous characterization techniques were applied in the investigation of material properties. Radioactive materials and radiochemical methods were used in the investigation of ion selectivities for europium and americium.

The materials were up to 400 times more selective towards europium over americium. For an application in nuclear fuel management, this order of preference is preferred, as americium can be readily recovered from the material for its fissioning, while europium is retained in the solid, a suitable matrix for nuclear waste disposal. In column operation, highly pure americium, up to 99.999 mol-%, could be separated from europium with high recovery in low pH. The effects of multiple factors on the separation, such as europium concentration, salt concentration and pH were investigated throughout the dissertation.

Ion exchange can excel in such specific and demanding jobs, as the structures of the materials can be engineered to enhance the desirable separation properties. Whereas the well-established solvent extraction based separation processes are already applied in many areas of nuclear fuel management, I believe that ion exchange can have a supportive role in their shortcomings.

Acknowledgements

The journey to finish my dissertation has been a long one. Albeit I have mostly worked in a solo project, I definitely could not have done it without all the support and ideas from our ion exchange research group, the iX group. The largest gratitude belongs to my supervisor and friend Dr. Risto Koivula, without your guidance I would have been lost multiple times. I feel our discussions were always constructive, albeit we though alike, sometimes too alike. Luckily, we had many group members around us to throw in new ideas or break the old ones. On this topic, special thanks to the two "thought factories": Wenzhong and Ilkka, together we had some wild ideas, not always (*ahem…*) related to the subject at hand. I am deeply grateful to my previous supervisor, Honorary Professor Risto Harjula, who is no longer with us. You were the one who set me on my path and always gave great support. I am also grateful to my early hands-on supervisor, Airi Paajanen, who guided me during my very first months.

I would like to thank all of our capable researchers in the iX group. Extended thanks to my closest co-workers and friends Junhua, Wenzhong, Ilkka, Satu and Valtteri. In addition to being able to work with you, I deeply appreciate our friendship! The iX group (www.helsinki.fi/ion-exchange) is a part of the wonderful research unit Radiochemistry at the Department of Chemistry, University of Helsinki. I owe great gratitude for our leadership, old and new, the professors Jukka Lehto, Anu Airaksinen and Gareth Law. I've always felt the right kind of leadership: when something needed to get done, it was, while otherwise we researchers had complete freedom to steer ourselves. Support was given whenever asked for and communication was never a problem for us. Additional thanks to the senior researchers I've got the most day-to-day support from, Maikki and Kerttuli!

The research summarised in this dissertation was funded by the State Nuclear Waste Management Fund, on the basis of proposals by the Ministry of Economic Affairs and Employment of Finland. It was a part of the Finnish Research Programme on Nuclear Waste Management which is based on the Nuclear Energy Act (990/1987). Big thanks to the personnel of the fellow projects inside the programme, especially to Silja Häkkinen and Kari Rasilainen of VTT, it has been a pleasure.

I am grateful to the support of my family, especially to the love of my life, my wife Suvi, who also *happens* to be a radiochemist!

"Nothing in life is to be feared, it is only to be understood."

- Marie Curie

Elmo Wiikinkoski,

Turku 2019

List of original publications

I. Wiikinkoski, E., Harjula, R., Lehto, J., Kemell, M., Koivula, R. (2017). Effects of synthesis conditions on ion exchange properties of α-zirconium phosphate for Eu and Am. *Radiochimica Acta*, 105(12), 1033. https://doi.org/10.1515/ract-2016-2740

II. Wiikinkoski, E., Xu, J., Zhang, W., Hietala, S., Koivula, R. (2018). Modification of α-Zirconium Phosphate Synthesis – Effects of Crystallinity and Acidity on Eu(III) and Am(III) Ion Exchange. *ChemistrySelect*, 3, 9583. https://doi.org/10.1002/slct.201801601

III. Wiikinkoski, E., Rautsola, I., Xu, J., Koivula, R. (2019). Column Separation of Am(III) and Eu(III) by α-Zirconium Phosphate Ion Exchanger in Nitric Acid.

The publications are found at the end of the thesis. They are referred to in the text by their roman numerals in bold.

The authors' contribution to the publications:

The research ideas were conceived by RK, RH and EW. The experimental design was done by EW and RK.

I-III are written solely by EW.

The exchangers were synthesized by EW in **I.** and by EW together with XJ and WZ in **II**.

EW carried out all of the experiments solely in **I**-**II,** and together with help from IR in **III**. Exceptions: SH performed the NMR analysis in **II**. MK and WZ performed SEM imaging in **I** and **II**.

Abbreviations

An	actinide(s)
BV	bed volume
CEA	Commissariat à l'énergie atomique et aux énergies alternatives
DIAMEX	diamide extraction
FESEM	field emission scanning electron microscope
FTIR	Fourier transform infrared transmittance spectroscopy
GANEX	group actinide extraction
HLW	high-level waste
ICP-OES	inductively coupled plasma optical emission spectrometry
Ln	lanthanide(s)
MAS NMR	magic angle spinning nuclear magnetic resonance
MP-AES	microwave plasma – atomic emission spectrometer
MA	minor actinides
NUEX	new uranium extraction
NEA	Nuclear Energy Agency
NPP	nuclear power plant
OECD	Organisation for Economic Co-operation and Development
P&T	partitioning and transmutation
PUREX	plutonium uranium redox extraction
XRD	powder X-ray diffraction spectroscopy
RR	research reactor
SANEX	selective actinide extraction
SNF	spent nuclear fuel
TRL	technological readiness level
TGA	thermogravimetric analysis
TRUEX	transuranium extraction
TBP	tributylphosphate
TALSPEAK	trivalent actinide lanthanide separation with phosphorous-reagent extraction from aqueous komplexes
ZrP	zirconium phosphate

Table of Contents

1 Introduction

1.1 The nuclear fuel cycle – open or closed?

Continuing political-technological debate in many countries is that of the future of their nuclear power. As research and hands-on experience on new spent nuclear fuel (SNF) reprocessing technologies pile up world-wide, the direct disposal of once-through SNF might not be the typical choice soon enough. The choice is not exclusive, of course. In many countries, the status is to study the impact of upcoming different technologies on their situation while currently the wastes are accumulated in interim storages. In some countries such as Finland, France and Sweden, considerable research effort is put into the safe disposal of SNF to the deep geological final repositories. In Finland, the operational licence will be applied for in the next few years, and in France and Sweden the commissioning is planned for around 2025 and 2030, respectively.

Most nuclear power countries consider the direct disposal of SNF, processed SNF, or other high-level wastes (HLW), while researching on the alternatives. A complementary fuel management route is the further reprocessing of SNF, dubbed partitioning and transmutation (P&T). For the countries involved in the Nuclear Energy Agency (NEA), the current strategies are compiled in Table 1.

Uranium and plutonium reprocessing is already well established and has been in commercial use for decades. After plutonium, the majority of long-term radiotoxicity and heat generation comes from the minor actinides (MA). What P&T offers is the further reduction of radiotoxicity by the transmutation of the MAs. The feasible factor of reduction is estimated to be 100-1000.[1,2] Transmutation refers to the incineration (fissioning) of target nuclides with both fast and thermal neutrons. Fast neutrons are preferred because of the high absorption of thermal neutrons leading to ineffective neutron economy.

The main goals of P&T are 1) the reduction of the radiological hazard in medium and long term, 2) the reduction of time in final storage to reach the reference level (the equilibrium radiotoxicity of the natural uranium required to fabricate the fuel) in radiotoxicity, and 3) the reduction in total waste volume.[2] All of these goals

increase the efficiency and lower the requirements of both interim storage and final disposal repositories.

Advanced partitioning is needed, because the most critical MAs, americium and curium, can be challenging to separate from the numerous fission products, namely the similar trivalent lanthanides. Their separation is required so that americium and curium can be transmuted without the hindrance from lanthanides. In past decades, many new technologies have been proposed for the partitioning of MAs, both aqueous and pyrometallurgical. This research is mostly state-driven because of the time and resources needed for such massive projects. Some technologies are individual element selective while others separate actinides from lanthanides as groups. Partitioning processes that purify Pu as a separate product bring an additional problem to the table: nuclear proliferation. Such is the case in conventional plutonium uranium redox extraction (PUREX) process. In upcoming technologies such as the French COEX™, the new uranium extraction (NUEX) or the group actinide extraction (GANEX) however, Pu is always recovered together with uranium or with multiple actinides.

Table 1. Strategies of NEA countries, India and China for handling their spent nuclear fuels from nuclear power plants (NPP) and research reactors (RR). Compiled from [3] with additions for Argentina, Finland and Romania.[4-6]

Country	Fuel type	Strategy
Argentina	NPP/RR	interim storage final strategy by 2030
Australia	RR	reprocessing abroad returning to supplier (US)
Austria	RR	returning to supplier (US)
Belgium	NPP/RR	reprocessing (earlier) no strategy (direct disposal considered currently)
Canada	NPP/RR	direct disposal as HLW
China	NPP/RR	reprocessing

Table 1 cont.		
Czech Republic	NPP/RR	direct disposal reprocessing (under consideration)
Denmark	RR	storage disposal abroad (if possible)
Finland	NPP/RR	NPP: direct disposal RR: returning to supplier (US)
France	NPP/RR	reprocessing
Germany	NPP/RR	reprocessing (stopped in 2005) direct disposal/ returning to supplier
Greece	RR	returning to supplier interim storage
Hungary	NPP/RR	no strategy on disposal long-term storage
India	NPP/RR	reprocessing
Italy	NPP/RR	reprocessing abroad (in France)
Japan	NPP/RR	reprocessing (can be revised)
Korea	NPP/RR	direct disposal (can be revised, not finally decided)
Mexico	NPP	no strategy
Netherlands	NPP/RR	reprocessing abroad (France) RR: disposal as HLW
Norway	RR	disposal reprocessing abroad
Poland	RR	returning to supplier no strategy for future management
Portugal	RR	returning to supplier
Romania	NPP/RR	direct disposal RR: returning to supplier
Russia	NPP/RR	reprocessing direct disposal (possible for some types)
Slovak Republic	NPP/RR	direct disposal reprocessing abroad

Table 1 cont.		
Slovenia	NPP	direct disposal or reprocessing abroad or multinational approach
Spain	NPP/RR	reprocessing up to 1983 direct disposal
Sweden	NPP/RR	direct disposal
Switzerland	NPP/RR	reprocessing not reprocessed SNF as HLW
Turkey	RR	reprocessing (as option – to be decided) direct disposal (as option – to be decided)
United Kingdom	NPP/RR	reprocessing direct disposal under consideration
United States	NPP/RR	reprocessing up to 1977 direct disposal as HLW (can be revised)

1.2 Separation technologies in spent nuclear fuel reprocessing

The technological readiness levels (TRL) of current technologies for processing nuclear materials were summarized by OECD-NEA in 2018.[7] The summary includes aqueous processes (Fig. 1), pyrometallurgical separation processes as well as head-end processes such as disassembly, fuel exposure and dissolution. Of the current technologies in use, the most matured for U and transuranium elements are based on solvent extraction with ion extracting reagents, whereas for Cs and Sr, on ion exchange materials. Technologies with the most progress are described in the following chapters.

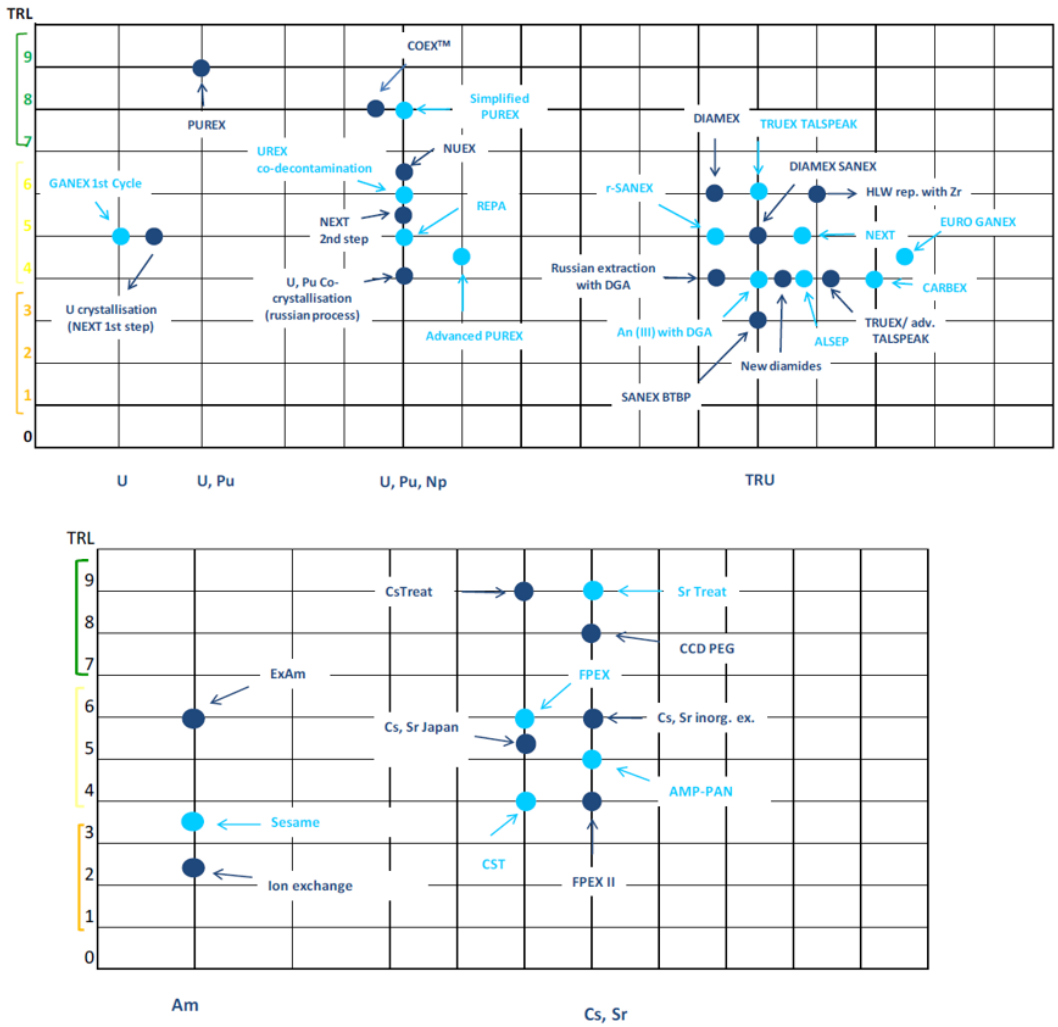

Figure 1. Summary of technological readiness levels (TRL) for aqueous processes. Reprinted with licence. Copyright © 2018, OECD.

1.2.1 Solvent extraction

For uranium based fuels, the PUREX process (TRL9, Fig. 1) has been dominating the reprocessing since its inception during the Manhattan Project in the 1940's.[8] In PUREX, the extraction of U(VI) and Pu(IV) is achieved by 30 vol-% tributylphosphate (TBP) in aliphatic hydrocarbons or their mixtures, e.g. in dodecane or kerosene. U(VI) and Pu(IV) are extracted from the strong nitric acid

aqueous phase as nitrate-TBP complexes into the organic phase, whereas fission products and tri- and pentavalent actinides Am, Cm and Np stay in the aqueous phase.

Since PUREX, numerous adaptations or new but similar technologies have been conceived. A common novel partitioning strategy, that follows the P&T concept, consists of the three following steps,[9] the last of which being arguably the most difficult:

i) Separation of U or U+Pu from dissolved SNF,

ii) Co-extraction of An(III)'s and Ln(III)'s and

iii) Separation of An(III)'s from Ln(III)'s.

New technologies have different approaches on the steps *i* to *iii*, and in some cases try to combine the steps. The separation of the similar An(III)'s and Ln(III)'s are made possible commonly through the use of soft-donor atom (N, S) containing complexants or extractants, which are selective for An(III)'s.[10-13]

The TALSPEAK (Trivalent Actinide Lanthanide Separation with Phosphorous-reagent Extraction from Aqueous Komplexes) process was conceived in the US in 1960's. It proposed the use of an extractant, with no selectivity between actinides or lanthanides, along with an actinide-selective holdback reagent DTPA (diethylenetriamine-*N*,*N*,*N*',*N*",*N*"-pentaacetic acid) added into either phase. TALSPEAK was never adopted due to its narrow applicable pH range and thus demanding control of feeds. It has however, "*inspired significant research activities dedicated to improving understanding of the basic chemistry that controls TALSPEAK (and related processes based on the application of actinide-selective holdback reagents)*", as Nash writes[14] in a recent comprehensive review on processes utilizing the TALSPEAK chemistry. The use of soft-donor atoms included in the their discussion, is the main important tool for any solvent extraction processes, as the ones briefly described in this chapter, that would separate An(III)'s from Ln(III)'s as groups.

The TRUEX (TRansUranium EXtraction) (TRL up to 6, Fig. 1) process for the co-recovery of both major and minor actinides from various types of highly acidic

nuclear waste solutions is based on the organophosphorous bifunctional compound, CMPO (Octyl(phenyl)-*N*,*N*-diisobutyl-carbamoylmethylphosphine-oxide), as the critical new extractant.[10,15] The extractant combination is 0.2 M CMPO and 1.2 M TBP in *n*-dodecane. High retention of tri-, tetra-, and hexavalent actinides from moderately acidic solutions and good selectivity over fission products are key features for CMPO. The relatively constant distribution values of Pu(IV), U(VI) and Am(III) between 1 to 6 M HNO_3 are of importance, as efficient extraction of actinides from dissolved fuels or wastes is then possible with little to no adjustment in the feed.

The COEX^{TM} (TRL8, Fig. 1) process, developed jointly by CEA and AREVA, for the purpose of enhanced proliferation resistance. Its main feature is the oxalic co-conversion is used to directly produce homogenous solid solution (U,Pu)O_2. Many parts of the PUREX process are adopted, with notable differences: *i*) no Pu is separated at any point in the process; *ii*) no Pu is stored in solid form and *iii*) the mixed oxide is directly fed from the conversion to mixed oxide fuel fabrication.[16]

The DIAMEX (DIAmide Extraction) (TRL6, Fig. 1) process is developed by the French CEA since 1980's for the extraction of actinides from nitric acid HLW solutions.[12] Diamides and malonamides, such as DMDBTDMA (*N*,*N*'-dimethyl-*N*,*N*'-dibutyltetradecylmalonamide) in commonly dodecane or toluene, have been proven suitable for the extraction of tri-, tetra- and hexavalent actinides from 4 M nitric acid or even stronger. Lanthanides are co-extracted.[17] Later, the DIAMEX-SANEX (TRL5, Fig. 1) counter-current process have been developed to follow the co-extraction of An(III)'s and Ln(III)'s by selective An-stripping by suitable reagents such as HDHP (di-*n*-hexyl phosphoric acid), to provide the separation.[18]

1.2.2 Ion exchange

Ion exchange was used for processing of nuclear fuels or wastes in the very beginning of the industry. Anion exchange resins were used for the clean-up of PUREX waste as they readily removed the fission products and TBP degradation products in the waste.[19,20] Historically most importantly, both cation and anion exchange have been used for concentration and purification for plutonium from the

isolated plutonium stream in PUREX. For that application, it competed with other proposed methods such as evaporation, precipitation and solvent extraction. Both cation and anion exchange could be used, but anion exchange proved superior. Plutonium was recovered from up to 8 M nitric acid by anion exchange resins. Cation exchange in turn was applied for more dilute PUREX streams.[21] Ion exchange was also applied for very specific tasks, such as the purification of uranium from ruthenium, or for the separation of neptunium from major actinides.[21]

Another major application of ion exchange in nuclear industry has been the purification of zirconium from the similar hafnium, which is always present along with zirconium. Whereas zirconium is ideal for nuclear applications due to its low neutron absorption, hafnium is the opposite. Zirconium is preferred by anion exchangers, while hafnium by cation exchangers. Despite the simplicity, ion exchange has since been replaced, for its lower efficiency, by solvent extraction and pyrometallurgical processes.[22]

In modern day when disposal of SNF and minimization of secondary radioactive waste volume are perhaps more carefully reassessed, there is cause to research on ion exchange again. Inorganic ion exchangers can offer inherent resistance to radiation, heat, and very acidic conditions. Because of their compact solid form, they are readily disposed of in repositories.

Setting the actinides aside, ion exchange has been also applied for fission product purification. Notably, for Cs and Sr, two major contributors to the radiotoxicity in medium term, in the nuclear energy environment. Since the nuclear incident in Fukushima in 2011, multiple contractors have been working on-site constructing and operating varying radioactive water treatment plants. The majority of radioactivity present in the stored waters is contributed by the fission products ^{137}Cs, ^{134}Cs and ^{90}Sr with half-lives between 2 to 30 years. Multiple purification approaches were combined in sequence, including co-precipitation, reverse-osmosis, and ion exchange, chelating resins, activated carbon, and other sorbents.[23] While other methods were first used to remove a major fraction of radioactivity, the high salinity in the waters hindered their progress. Extremely selective ion exchangers were applied in the later stages of the processes for the

remainder. The ion exchangers used can be divided into four types: zeolites (microporous aluminosilicates), hexacyanoferrates, silicotitanates and titanates. The hexacyanoferrate CsTreat® (TRL9, Fig. 1) was previously proven in highly saline waste in industrial scale in Loviisa power plant in Finland since 1990's, and the sodium titanate SrTreat® (TRL9) has been first used in industrial scale for removal of strontium from process water in Murmansk, Russia, in 1990, hence their high TRL's.[23]

1.3 The *f*-elements

The lanthanides (Ln) are the 15 metals from lanthanum to lutetium, and make up the so called rare-earth elements together with scandium and yttrium. Chemically, all lanthanides behave in a similar way and successive addition of an electron to one of the seven 4*f* orbitals is characteristic of the lanthanide series. The full 6*s* and 5*p* electrons are further away from the nucleus than the 4*f* electrons, so in lanthanides apart from Ce, 4*f* electrons do not take part in bond forming. Loss of electrons from the 6*s* and 5*p* orbitals results in lanthanide ions, most common oxidation state being +III. The ionic size decreases with increasing atomic number. The phenomena is known as the lanthanide contraction. As atomic number is increased along the series, the nuclear charge grows. However, additional electrons populate the poorly shielding *f*-orbitals and do not increase the radius of the electron cloud. In turn, increased charge in the nucleus contracts the cloud. The ion radius affects the lanthanides ability to solvate, hydrolyse and form complexes and many intra-lanthanide separation processes utilize these differences.[24]

The actinides (An) are the 15 metals from actinium to lawrencium. They are all radioactive elements with no stable nuclides. Similarly to the gradually filling 4*f* orbitals for lanthanides, the actinides are characterized by the analogous filling of 5*f* orbitals. The quite extensive similarity between the An and Ln series arises from this analogy in electron configuration, however, actinide chemistry is far more complex. Actinides can be divided into naturally occurring light actinides, and to transuranic elements (Np, Pu, Am, Cm) which are produced in nuclear reactions. In addition to the electron configuration of [Rn], the actinides have variable amounts of electrons on the 5*f*, 6*d* and 7*s* orbitals. The 5*f* electrons are closer to the nucleus

than the 6*d* and 7*s* electrons, however the energy differences are very small. Due to this, in lighter actinides up to americium, also the 5*f* electrons take part in chemical bonding. For this reason the chemical behaviour of the actinides is more complex than that of the lanthanides. The chemistry of the lighter actinides up to plutonium resemble more that of *d*-transition elements, as they readily form complexes and covalent bonds. The compounds of heavier actinides are mostly ionic, similar to lanthanides. The oxidation states of the actinides can vary between +II and +VII, and the ionic radii in the same oxidation state decreases along with increasing atomic number: the actinide contraction.[24]

The natural, safe lanthanides are often used as analogues for applicable actinides in experiments. Thus the use of radioactive materials can be minimized if not avoided. Such an approach does not apply for the work presented in this thesis. On the contrary, in this case the aim is to purposefully exploit the slight differences in europium and americium, the two very similar elements of which europium is traditionally used as a chemical analogue for americium.

The electron configurations for the europium and americium atoms are [Xe]$4f^7 6s^2$ and [Rn]$5f^7 7s^2$ and for the +III ions [Xe]$4f^6$ and [Rn]$5f^6$, respectively. The Shannon effective ionic radii for europium(III) and americium(III) are 94.7 pm and 97.5 pm for coordination number 6, respectively, and 106.6 pm and 109 pm for coordination number 8, respectively.[25]

1.4 Zirconium phosphates

Zirconium phosphates (ZrP) have been studied as cation exchangers, catalysts or catalyst supports,[26-30] proton conductors in fuel cells,[31-34] hydrogen storage,[35] drug delivery systems[36,37] and surface modified multifunctional materials.[38] In ion exchange, wide variety of studied target elements include cations from all sizes and varying valences: alkali metals from Li to Cs,[39-42] Ba, Y and La,[43] Co, Nd and Dy[44-46] and Eu and Am[47-50], including some radioactive applications for Cs, Eu and Am. Their applications were significantly increased by the discovery of inorganic-organic zirconium phosphonate chemistry, however the subject is out of scope for this text. Because the phosphonate group

can be selected among numerous varieties, the configurations of different possible zirconium phosphate-phosphonates are endless and can be very complicated.

Numerous zirconium phosphate crystal structures are known: $Zr(HPO_4)_2 \cdot H_2O$ (hence α-ZrP),[51] $Zr(PO_4)(H_2PO_4) \cdot 2\ H_2O$ (γ-ZrP),[52,53] $Zr(HPO_4)_2$ (τ-ZrP and τ'-ZrP),[54,55] and $Zr(HPO_4)_2 \cdot 8\ H_2O$ (θ-ZrP).[56,57] The α, γ and θ phases are layered structures with crystalline water in interlayer space, whereas the τ and τ' phases are anhydrous 3D structures. In the thesis, only the α phase will be focused on.

In α-ZrP, a layer consists of zirconium atom plane that resides between two planes of monohydrogen phosphates. The monoclinic crystal structure has the space group $P2_{1/c}$. Each Zr is coordinated octahedrally to one oxygen atom of each six surrounding phosphate groups (Fig. 2a). The OH groups are pointed towards interlayer space and alternate with the OH groups from the next layer. Staggered adjacent layers create cavities, which contain the crystalline water (Fig. 2b). Leading to the cavities, the largest openings are 2.62-2.64 Å as reported by Clearfield.[58]

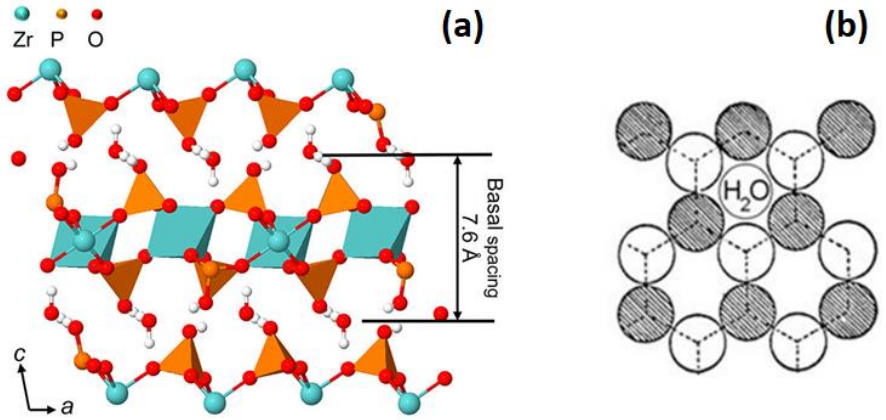

Figure 2. (a) Structure of α-ZrP. Modified and reprinted with permission, from Cheng et al. *Inorg. Chem.* 2018, 57, 8, 4370-4378. Copyright © 2018, American Chemical Society. (b) Schematic of OH groups of two adjacent layers, dark and light, forming cavities in the interlayer plane, wherein reside the crystal water molecules. Reprinted under Creative Common licence, from Casciola, *Solid State Ionics* 2019, 336, 1-10.

It has been discussed[58,59] that narrow openings limit the ion exchange capabilities and hinder the kinetics in α-ZrP. The structure is sturdy and will not easily swell in pure water. However, the structure is further hydrated by acid treatment, and the resulting θ-ZrP with 8 crystalline water molecules has an increased interlayer distance (from 7.6 Å to 10.4 Å).[56] Alternatively, the hydrogen in α-ZrP can be exchanged with ions such as ammonium, sodium or potassium to increase the interlayer distance to 9.5, 10.0 or 10.8 Å, respectively.[51]

Zirconium phosphates can be synthesized in a plethora of ways. Most simply, by just adding a source of dissolved zirconium(IV) into a phosphoric acid in the correct conditions, as zirconium phosphate is very stable. However, to create pure and crystalline product, the story is not so straightforward. Both the crystal size and morphology of ZrP materials can be affected in numerous ways, by tuning the reagents, their concentrations, the temperature, time or solvents, or by a suitable post-synthesis treatment.[55,60-62]

The zirconium phosphate gels can be produced by dissolving zirconium tetrachloride, or more commonly zirconium oxychloride octahydrate, in hydrochloric acid. The solution is then added slowly to phosphoric acid. The gel can then be washed, dried and used as-is, or properly made into crystalline material through steps like rigorous refluxation, up to weeks.[51,63] Another pathway to highly crystalline ZrP are the hydrothermal methods, and the so-called HF method, which cleverly utilized the complexation of Zr by fluorine and subsequent slow evaporation of it, resulting in slow growing ZrP crystals.[64] Now, more focus is given on HF-free methods as per its toxicity. Recently, new interest arises in zirconium phosphate for the mentioned numerous applications. According to the times, green and minimalistic methods are applied also to the ZrP synthesis. Cheng et al. has proposed a sustainable, HF-free, atom economic, minimalistic and scalable route to highly crystalline ZrP, of a selected particle size from nano to micrometres.[59,65]

2 Aim

Aim of the study was to create inorganic ion exchange material for the purpose of An(III)/Ln(III) separations. The materials would be used in columns, preferably in simple mineral acids without addition of multiple reagents, organic or otherwise. The research effort was started with the idea of screening of multiple phosphates, such as ammoniummolybdophosphates, zirconium, titanium and hybrid zirconium-titanium phosphates, to see the extent of their separation capabilities using model elements Eu(III) and Am(III). The idea to screen phosphates originally came from the solvent extraction: if phosphate bearing reagents work for them in these applications, why not for us.

As zirconium phosphate was quickly found to be promising, the research effort was focused on it. After preliminary studies in plain nitric acid or nitric acid with background electrolytes, a new question arose: How could we further improve the separation, without making the *solution* more complex? Thus, the material study was started. Multiple different routes to create zirconium phosphates were adapted from the literature, with the aim to correlate changes in the exchanger material with changes in the ion exchange properties and separation capability (papers **I** and **II**), and all this was a planned gateway to most optimal column separation (paper **III**).

3 Experimental

3.1 Theory and equations

Throughout the experimental part of the thesis, quantities, such as selectivity coefficient, distribution coefficient, metal binding coefficient and acid dissociation constant, are calculated. In this chapter is the compilation of the theory and equations that were used throughout the appended publications, all based on the works of Helfferich and Harjula.[66,67]

A binary exchange reaction between ions $\mathrm{A}^{Z_\mathrm{A}}$ and $\mathrm{B}^{Z_\mathrm{B}}$ may be expressed as

$$z_\mathrm{B}\mathrm{A}^{Z_\mathrm{A}} + z_\mathrm{A}\overline{\mathrm{B}}^{Z_\mathrm{B}} \rightleftharpoons z_\mathrm{B}\overline{\mathrm{A}}^{Z_\mathrm{A}} + z_\mathrm{A}\mathrm{B}^{Z_\mathrm{B}} \quad (1)$$

where the barred symbols refer to the ions in the solid phase, and z_A and z_B are the respective ion charges. The **selectivity coefficient** $k_{A/B}$ for the reaction can be written as

$$k_{A/B} = \frac{[\bar{A}]^{z_B}[B]^{z_A}}{[A]^{z_B}[\bar{B}]^{z_A}} \quad (2)$$

where [A] and [B] refer to the ion concentrations in the solution and corresponding barred symbols refer to the concentrations in the exchanger phase. The **distribution coefficient** K_d of ion A is defined as

$$K_d = \frac{[\bar{A}]}{[A]} \quad (3)$$

Combining Eqs. 2 and 3 gives the relation between the distribution coefficient and the selectivity coefficient

$$K_d{}^{z_B} = k_{A/B}\frac{[\bar{B}]^{z_A}}{[B]^{z_A}} \quad (4)$$

In the case that A is present in trace concentrations ($[\bar{A}] \ll [\bar{B}]$ and $[A] \ll [B]$), the concentration of B in the exchanger is practically constant and equal to the ion exchange capacity *Q* of the exchanger ($[\bar{B}] \approx Q$). Under these conditions, one obtains in logarithmic form[66]

$$\log K_d = \frac{1}{z_B}\log\left(k_{A/B}\, Q^{z_A}\right) - \left(\frac{z_A}{z_B}\right)\log [B] \quad (5)$$

i.e. the plot of $\log K_d$ vs. $\log[B]$ is a straight line with a slope of $-(z_A/z_B)$. These conditions applied throughout the work that included carrier free radioactive tracers, as the concentrations for Am and Eu (A) were in the order of 10^{-9} to 10^{-11} mol·L^{-1}, were much lower than those of the hydronium ion (B), 10^{0} to 10^{-3} mol·L^{-1} in pH 0 to 3.

The distribution coefficient (K_d) can be experimentally determined from

$$K_d = \frac{\text{radioactivity concentration in exchanger}}{\text{radioactivity concentration in solution}} = \frac{A_0 - A}{A} \times \frac{V}{m} \quad (6)$$

where A_0 is the initial solution radioactivity and *A* is the solution radioactivity at equilibrium. *V* is the volume of the solution, *m* is the mass of the exchanger and the ratio of these two is called the batch factor (*V/m*).

Like orthophosphoric acid, zirconium phosphate is weakly acidic in nature, and the dissociation of the OH groups attached to the phosphorus atom can be characterized by the **acid dissociation constant** K_a:

$$\frac{[PO^-][H^+]}{[POH]} = K_a \quad (7)$$

and

$$pK_a = -\log K_a \quad (8)$$

where $[POH]$ is the concentration (mmol·g^{-1}) of undissociated phosphorous OH groups in the material and $[PO^-]$ is that of the dissociated ones. $[H^+]$ refers to hydronium ion concentration in the water inside the pores of the solid material and may not necessarily be that of the external solution.[67]

The degree of dissociation (β)

$$\beta = \frac{[PO^-]}{[POH] + [PO^-]} \quad (9)$$

depends on pK_a and pH according to Helfferich[67]:

$$\log\frac{1-\beta}{\beta} = pK_a - pH \quad (10)$$

Thus, at 50% dissociation (β = 0.5)

$$pK_a = pH \quad (11)$$

In titration with NaOH, the charge of the PO^- groups in the material will be balanced by the Na^+ ions:

$$POH + NaOH \rightleftharpoons PONa + H_2O \quad (12)$$

The total ion exchange capacity (Q) of the material is thus

$$Q = [POH] + [PONa] \quad (13)$$

The inherent acid character of the materials in H-form affects the pH upon immersion in water. When alkali is added to the system in the form of dilute NaOH solution, pH increases characteristic to the material in question. Based on Eq. 12

and taking into account the autodissociation of water, the **conversion to the Na-form** (q_{Na}, meq·g^{-1}) can be calculated from

$$q_{\mathrm{Na}} = ([\mathrm{OH^-}]_{\mathrm{i}} - [\mathrm{OH^-}] + [\mathrm{H_3O^+}] - [\mathrm{H_3O^+}]_{\mathrm{i}})(V/m), \tag{14}$$

where $[\mathrm{OH^-}]_{\mathrm{i}}$ refers to the added hydroxide and $[\mathrm{H_3O^+}]_{\mathrm{i}}$ to the initial pH before addition. $[\mathrm{OH^-}]$ and $[\mathrm{H_3O^+}]$ are calculated from pH measured after equilibration.

The selectivity coefficient as formulated in Eq. 2 contains two reactions. First, the dissociation of the OH group; i.e.

$$\mathrm{POH} \rightleftharpoons \mathrm{PO^-} + \mathrm{H^+} \tag{15}$$

Second, binding of the metal in the PO$^-$-group, i.e.

$$3\,\mathrm{PO^-} + \mathrm{M^{3+}} \rightleftharpoons \mathrm{M(PO)_3} \tag{16}$$

which can be characterized by the **metal binding coefficient** k_{M}

$$k_{\mathrm{M}} = \frac{[\mathrm{M(PO)_3}]}{[\mathrm{PO-}]^3[\mathrm{M^{3+}}]} \tag{17}$$

or by using notation of Eq. 2,

$$k_{\mathrm{M}} = \frac{[\overline{\mathrm{M^{3+}}}]}{[\mathrm{PO-}]^3[\mathrm{M^{3+}}]} \tag{18}$$

Using similar notation for K_{a} (in Eq. 7, [POH] = $\overline{\mathrm{H}}$) and combining Eqs. 2, 7 and 17 it can be seen that

$$k_{\mathrm{M/H}} = K_{\mathrm{a}}^3\, k_{\mathrm{M}} \tag{19}$$

and finally, in logarithmic form:

$$\log k_{\mathrm{M}} = \log k_{\mathrm{M/H}} + 3\, pK_{\mathrm{a}} \tag{20}$$

The **crystallite size** L in a powderous crystalline material can be calculated based on X-ray diffraction pattern from

$$L = \frac{K\lambda}{\beta \cos\theta}, \tag{21}$$

where K is the shape constant, λ is the wave length of radiation used, and β is the full-width at half maximum (in radians) of the peak at an angle θ. The calculation holds true for crystallites in the nanoscale. [68,69]

3.2 Brief strategy behind the experiments

For Paper **I**, varying synthesis routes for ZrPs were tested with separation capability for Eu and Am already in mind from the start. Effects of material properties on ion exchange properties were discussed. Some trends and correlations among the three products were reported. As the routes were largely different however, even in the reagents and the post synthesis treatment, the reasons for the variation in the sorption properties were left unclear. For that, the next Paper **II** was designed to have just one variable in the synthesis: reflux time for crystallization. Thus, a single one-pot synthesis was carried out, with aliquots of the reaction mixture evacuated at five-fold time intervals. The aliquots were then treated equally, and the resulting three products thoroughly investigated. For Paper **III**, the earlier knowledge was combined and a promising product among the six was selected for further batch experiments, and final column separations.

3.3 Materials and instrumentation

Analytical grade reagents and other chemicals were supplied by Sigma-Aldrich and Merck Millipore. The water used throughout the work was distilled and purified (18.2 MΩ, Millipore Milli-Q water purification system). In synthesis, borosilicate glassware and ceramics were used. In batch experiments, polyethylene vials were used. In analysis, polypropylene with polyethylene centrifuge tubes were used. In material digestion, Teflon containers were used. In column operation, low-pressure Econo chromatography columns (Bio-Rad) consisting of borosilicate glass, polypropylene, and polyethylene were used along with Tygon tubing. The carrier-free tracers ^{241}Am(III) and ^{152}Eu(III) were obtained from New England Nuclear Corporation and Amersham Plc., respectively.

Radiometric analysis was done with PerkinElmer-Wallac Wizard 1480 gamma counter equipped with NaI detector, and with Canberra high purity germanium (HPGe) gamma spectrometer, with 45% relative efficiency, equipped with Genie2000 software.

Inactive Eu(III) analysis was carried out with Agilent MP 4200 microwave plasma – atomic emission spectrometer (MP-AES) equipped with an SPS 3 autosampler. La was used as an internal standard for quality control and Cs as an ionization buffer.

X-ray diffraction patterns were recorded with Philips PW1820 powder diffractometer equipped with Philips PW1710 control unit and Siemens Kristalloflex X-ray generator. Copper K_α X-rays of wavelength 1.54056 Å were used along with 2θ angle step size of commonly 0.010 to 0.040° and counting rate of commonly 2.5 to 10 seconds per step, over the total 2θ range of commonly 4 to 70 or 7 to 70°. Unit cell parameters were calculated using UnitCell software developed by Tim Holland and Simon Redfern.[70]

Solid-state ^{31}P magic angle spinning nuclear magnetic resonance (^{31}P MAS NMR) spectra were obtained with a Bruker Avance III NMR spectrometer operating at 500 MHz for protons. Bruker high power decoupling pulse sequence with proton decoupling was used for measurements, and the spectra were externally referenced to 85% H_3PO_4.

For morphology imaging, Hitachi S-4800 field emission scanning electron microscope (FESEM) was used. For some of the materials, the P:Zr ratios were measured with an Oxford INCA 350 energy dispersive X-ray spectrometer (EDX) connected to the electron microscope. Powderous samples were attached to a carbon tape and excess particles were removed by pressurized air flow and coated with gold-platinum alloy.

For elemental analysis from digested ZrP samples, PerkinElmer Optima 8300 inductively coupled plasma optical emission spectrometer (ICP-OES) was used in dual view, with a GemTip CrossFlow II nebuliser, a Scott Spray Chamber Assembly, a sapphire injector and a HybridXLT ceramic torch. Lanthanum was used as an internal standard for quality control.

Thermogravimetric analysis (TGA) was done with Mettler Toledo TGA system with STARe software. The used temperature program consisted of constant heating commonly at the rate of 2 or 10 °C·min^{-1} from commonly 25 °C to 800 °C under nitrogen gas flow.

Infrared transmittances were measured with *i*) Bruker Alpha-P FTIR instrument fitted with a diamond ATR sampling accessory, or with *ii*) Spectrum One FTIR spectrometer (PerkinElmer) fitted with Universal ATR sampling accessory and Spectrum software. Commonly wavenumbers from 4000 to 400 cm^{-1} were recorded.

3.4 Methods

The determination of distribution coefficients (K_d) in batch was the most common type of experiment throughout the thesis work. The K_d's for Eu and Am were determined as function of pH, salt concentration, the concentration of each other, or time. In these experiments, a set amount of a ZrP product was equilibrated for 3 days with a given solution, in a slow rotary table (10 rotations per minute). The supernatant was separated by filtration and its radioactivity was measured. The K_d was determined according to Equation 6. The batch factor (V/m) was always 500 $L \cdot kg^{-1}$, as the mass was always 20 mg and the solution volume 10 mL. Commonly three full procedure repetitions were conducted for an experiment. Instead of the *initial radioactivity* in Equation 6, method blank radioactivity was used. Method blank is the same as an actual sample but without any added exchanger and goes through all of the steps in the procedure. Comparing this with the sample increases the validity of the result: as some of the analytes are always lost by other means than sorption to the investigated material, e.g. to the vial walls, the cap or the filter, the same amounts are lost in the method blank. Thus, only the effect of the sorbent is affecting the K_d.

Titration experiments were done by the addition of strong sodium hydroxide to vials with 20 mg studied exchangers and 10 mL pure water. The base was added in small increments, and the samples were equilibrated always for one day in a slow rotary mixer. pH was then recorded from the supernatant, before the next cycle began with the next addition.

In column operation, commonly 1 mL bed volume (BV) was used. The exchanger was wetted in dilute nitric acid and the slurry was transferred with a disposable pipette to the column. Flow direction was top-down, and the solution was pumped

with a peristaltic pump set before the column, commonly with a rate between 5 and 15 $BV \cdot h^{-1}$. After packing, the materials were always first conditioned with a stronger nitric acid to ascertain H-form before the start of the experiment. Throughout the column experiments, the packed material was never left to dry to avoid problems: small amount of the preceding solvent was always left on top of the material when changing solvents. Automatic fraction collectors were used to gather the eluate in small fractions, commonly >5 to 10 mL, in 15 mL tubes. From the fractions, aliquots were pipetted to produce measurement preparates for radiometric (gamma counting), or spectrometric (MP-AES) determinations.

In elemental analysis, ZrP products were digested in a microwave assisted digestion system. Samples of approx. 15 mg were placed in a mixture of concentrated nitric acid (65%; 10 mL) and hydrofluoric acid (40%; 0.25 mL) in sealed containers. No residue was left after the procedure. Measurement preparates were produced by dilution and the Zr and P concentrations were quantitatively determined by ICP-OES.

3.5 Synthesis

Several syntheses were carried out to acquire α-ZrP's of varying crystallinity and acidity. These sol-gel syntheses are summarized in Table 2. In general, a heated aqueous phosphate solution (B) was drop-wise added to a heated aqueous zirconium solution (A) in a round-bottom flask with constant stirring. The resulting gel was then refluxed in the same conditions for a variable amount of time, followed by the separation from mother liquor in a centrifuge, numerous washing procedures and drying in mild conditions. The series of ZrP1, ZrP5 and ZrP25 were done all together in one-pot synthesis. The gel was prepared and the reflux started, and after 1 and 5 hours had passed, approx. 1/3 fractions of the product were evacuated from the flask. The final 1/3 was refluxed for 25 hours, total. Subsequently and immediately after each evacuation, the three product fractions were treated equally in all aspects. In all of the cases, the final products were then ground and sieved, and the only particles between 75 and 150 µm were used for experiments.

Table 2. Summary of synthesis procedures for all of the zirconium phosphates products involved in the text.

Label (paper)	Preparation of gel	Additional steps	Washing	Drying
ZrPA (I)	A: 400 mL of 1.25 M H_3PO_4 B: 25 g $ZrCl_4$ in 430 mL 2 M HCl	None	0.3 M H_3PO_4 until pH levelled off	At room temp.
ZrPB (I)	A: 11 g $ZrCl_2{\cdot}H_2O$ in 160 mL B: First 8 mL 40% HF, second 92 mL 85% H_3PO_4	Left overnight under airflow to evaporate HF	0.3 M H_3PO_4 until pH levelled off	At room temp.
ZrPC (I)	A: 6.4 g $ZrCl_2{\cdot}H_2O$ in 20 mL water at 80 °C B: 55 g $NaH_2PO_4{\cdot}H_2O$ in 40 mL 3 M HCl at 80 °C	Reflux at 80 °C for 30 hours, precipitate left in mother liquor for 2 days, at room temp.	1. 2 M H_3PO_4 2. water until pH 3	4 days at 60 °C
ZrP1 (II)	A: 16.1 g $ZrCl_2{\cdot}H_2O$ in 50 mL water at 80 °C B: 138 g $NaH_2PO_4{\cdot}H_2O$ in 100 mL 3 M HCl at 80 °C One preparation for the three products together	Reflux at 80 °C 1/3 evacuated after 1 hour	1. 2 M HCl 2. 2 M H_3PO_4 3. water until pH 3	3 days at 60 °C
ZrP5 (II)		1/3 evacuated after 5 hours	same as above	3 days at 60 °C
ZrP25 (II, III)		The remainder evacuated after 25 hours	same as above	3 days at 60 °C

4 Results and Discussion

4.1 Chemical and structural analysis

To support the Eu-Am separation studies conducted with various ZrP products, and to give reason for the differences found in ion exchange properties between the studied products, it was necessary to carefully characterize the materials on their structure, composition, morphology and chemical properties. Powder X-ray diffraction spectroscopy (XRD) was utilized for structural insight. The composition was determined combining elemental analysis, thermogravimetry and ^{31}P MAS NMR. The morphology was studied by SEM. Further, the acid character and the ion exchange capacity were determined by titration.

4.1.1 Characterization of the solid powders

Powder XRD studies shows that all samples contain the α phase with the 002 reflection at approx. 11.7° (2θ) that corresponds to the interlayer distance, 7.6 Å (Fig. 3). No detectable amount of γ, τ, τ' or θ phases for which the main peaks would appear at 7.2° (12.2 Å), 15.7° (5.6 Å), 15.9° (5.6 Å) or 8.6° (10.4 Å), respectively, were found.[51,54,55,57]

For the product series presented in paper **II**, Scherrer crystallite sizes were approximated from the powder X-ray data based on the Scherrer equation (Equation 21) that is valid for crystals and crystallites in the nanoscale.[68,69] The crystallite size approximately doubles during the series ZrP1 to ZrP5 to ZrP25, roughly in order of 10 to 15 to 20 nm. Meanwhile, particle size greatly decreases, so that in ZrP25 the particle size is similar to the crystallite size. In summary, the "less crystalline" products have nanocrystallites aggregated together creating big micrometre scale clumps of material, and in the most crystalline, the particles are effectively separate nanosized crystals.

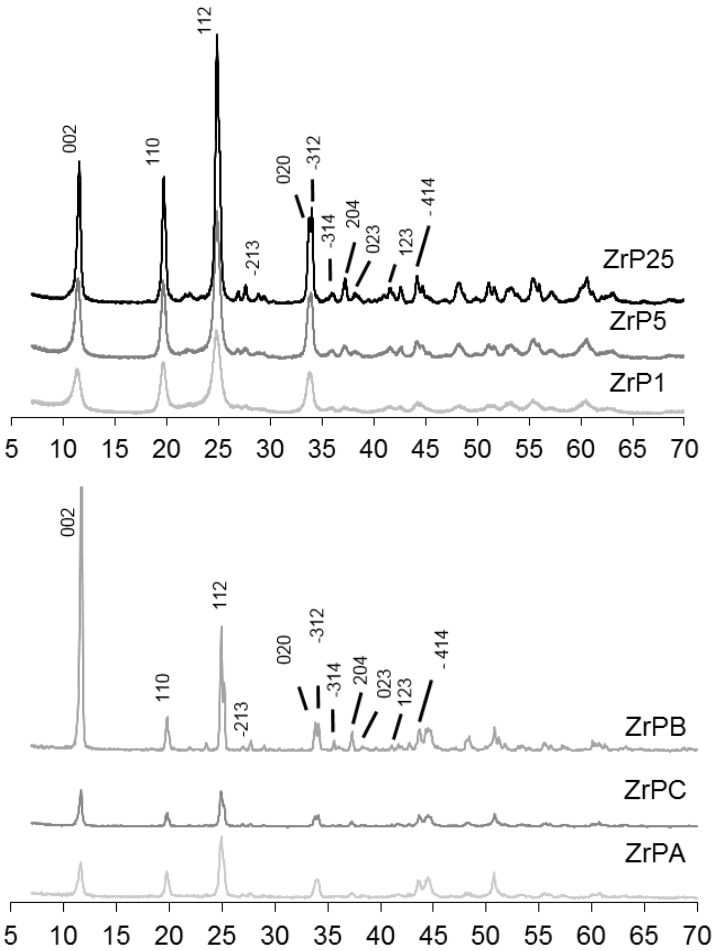

Figure 3. The powder X-ray diffraction patterns of the six synthesized ZrP products. Intensity (in arbitrary units) as a function of 2θ angle. For ZrPB, the first peak is cut off. The intensities of the first peaks are 12:2:1 for ZrPB:ZrPC:ZrPA, whereas the intensities of the background in the surrounding regions are 1:1:1. Miller indices are labelled on top of the most intensive reflections.

The morphologies were investigated with FESEM. The most crystalline products (ZrPB, ZrPC, ZrP25) exhibit hexagonal plate-like structures (Fig. 4) familiar to a certain extent to the perfect hexagonal plates seen in highly crystalline α-ZrP.[44] The less crystalline product ZrPA has similar plate-like features, but the plates are aggregated or 'glued' together in varying orientations by a continuous phase in between, forming massive particles in comparison. The least crystalline products (ZrP1, ZrP5) are big clumps of material with a wave-like fine structure on their surfaces, which still could correspond to edges of the similar plate-like features.

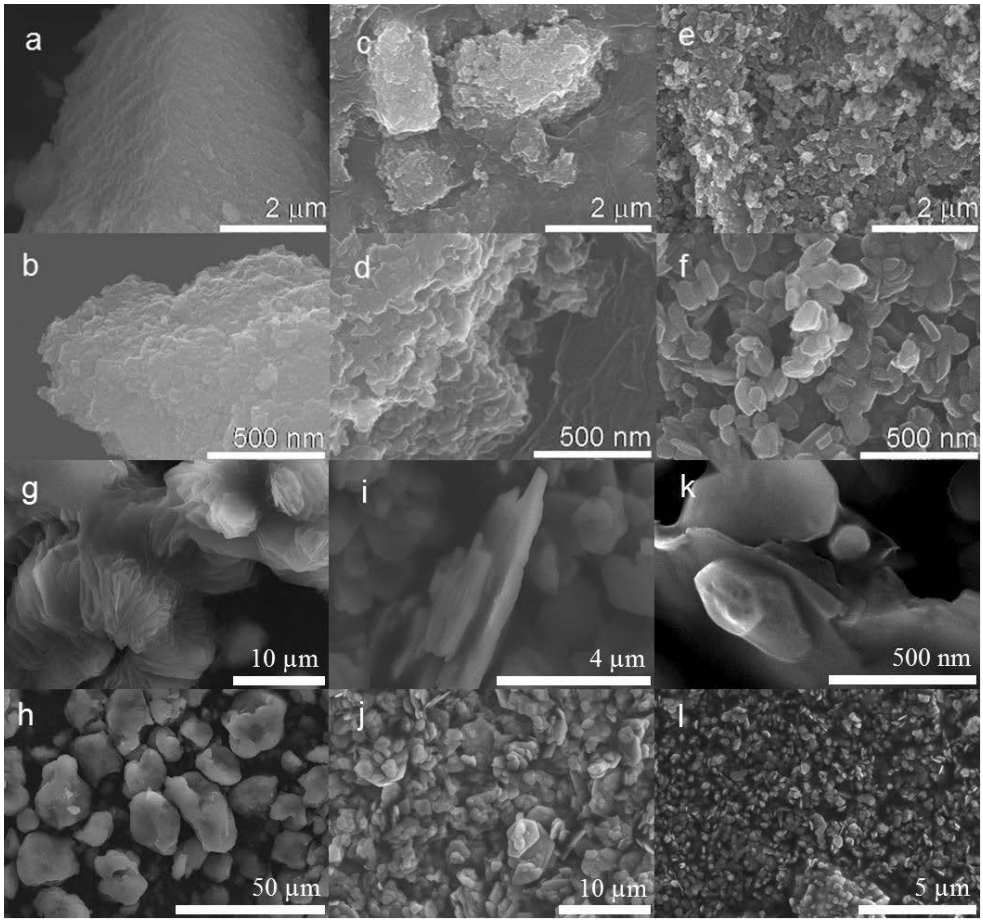

Figure 4. The morphology of the ZrP particles as imaged with a Hitachi S-4800 field emission scanning electron microscope. (a,b) ZrP1, (c,d) ZrP5, (e,f) ZrP25, (g,h) ZrPA, (i,j) ZrPB, (k,l) ZrPC.

The solid-state ^{31}P MAS NMR technique has been previously applied for zirconium phosphate and analogous titanium phosphate research to distinguish the crystallographically different phosphate groups. In the α-structure, each monohydrogen phosphate group HPO_4^{2-} is bound to three Zr atoms and has the resonance in the region of -18.7 to -22.8 ppm, in reference to 85% orthophosphoric acid. In pure and crystalline α-structure, only this type of phosphate groups are present. Resonances between -14.8 to -15.0 ppm correspond to $H_2PO_4^-$ bound to

two Zr atoms and resonances between -27.4 ppm to -28.3 ppm correspond to PO_4^{3-} bound to four Zr atoms.[71-75]

This technique was applied for the materials presented in paper **II**. In ZrP1, where the least time was given for the α-crystals to form, the majority of phosphate is of the type of type HPO_4^{2-}, however, the other two types are present in a lesser degree. In ZrP5 and ZrP25, neither $H_2PO_4^-$ nor PO_4^{3-} are present (Fig. 5). The NMR data was deconvoluted and quantified, and through the combination of the NMR technique, thermogravimetric analysis and elemental analysis, chemical compositions were determined. ZrP1: $Zr(H_2PO_4)_{0.08}(HPO_4)_{1.87}(PO_4)_{0.06} \cdot 0.66\ H_2O$, ZrP5: $Zr(HPO_4)_2 \cdot 0.48\ H_2O$ and ZrP25: $Zr(HPO_4)_2 \cdot 0.55\ H_2O$. Details for the calculations are available in the supporting information for paper **II**.

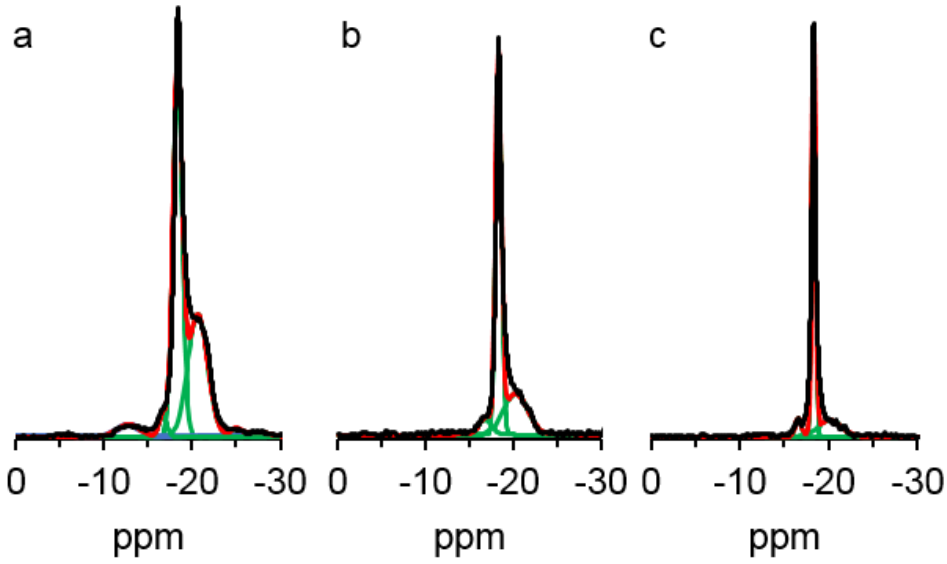

Figure 5. Solid-state ^{31}P MAS NMR spectra of the ZrPs in reference to 85% orthophosphoric acid in ppm: a) ZrP1 b) ZrP5 c) ZrP25. Six significant peaks for were found for ZrP1 and taken into account in calculations: -13 ppm ($H_2PO_4^-$); -16, -18 and -21 ppm (HPO_4^{2-}); -25 and -27 ppm (PO_4^{3-}), peak designations in parentheses. Three for ZrP5 and ZrP25: -16, -18 and -21 ppm. Reproduced with licence from Wiikinkoski et al. *ChemistrySelect*, 2018, 3, 9583.

4.1.2 Acid dissociation constant

The acid character of the products, namely the first acid dissociation constant pK_{a1}, was determined through Na conversion, i.e. titration with NaOH. For the titrations done in paper **I**, there was Na already present in the electrolyte solutions, as the titrations were done in the conditions of the ion exchange experiments. Thus the values attained for pK_{a1} in the paper **I** are called *apparent pKa in experimental conditions*. For the paper **II**, the titration was done in pure water, giving the actual pK_{a1} of for the materials. It is clear that having sodium already present releases additional hydrogen via ion exchange, and a lower pH is measured, resulting finally in a lower than true pK_{a1} value.

Although in the structure we can see only equivalent POH groups, it is clear from the titration curves (Fig. 6) that the materials have two equivalence points, as if the material was a diprotic acid, corresponding to its chemical formula. In the bulk material there are twice as many P than Zr, but since each Zr is symmetrically surrounded by six POH groups, there is no distinction as to which specific two POH groups are associated with a specific Zr atom. Combining these facts with the features of the titration curves, it must mean that when one hydrogen is exchanged for a metal, the acid character of *a nearby* POH group, or groups, is altered.

Sodium conversion was calculated from equation 14. The pK_{a1} values were graphically attained from the first plateau, midway to the first equivalence point (equations 9-11). In similar manner, the second acid dissociation constants could be obtained from between the two equivalence points. Only the first dissociation constant were considered in all of the papers, because both the experiments and the possible applications are always in the very low pH, and for low capacity use, wherein the remaining hydrogens corresponding to pK_{a2} perhaps are not utilized at all. Though because of the extreme preference for M^{3+} over H^{+} the possibility cannot be ruled out completely.

The *apparent* pK_{a1} values, in sodium nitrate solution, for the materials ZrPA, ZrPB and ZrPC are 3.5, 2.3 and 3.1, respectively. The pK_{a1} values for the materials ZrP1, ZrP5 and ZrP25 are 6.1, 6.3 and 6.9, respectively, while their pK_{a2} values are roughly from 8.5 to 9.5.

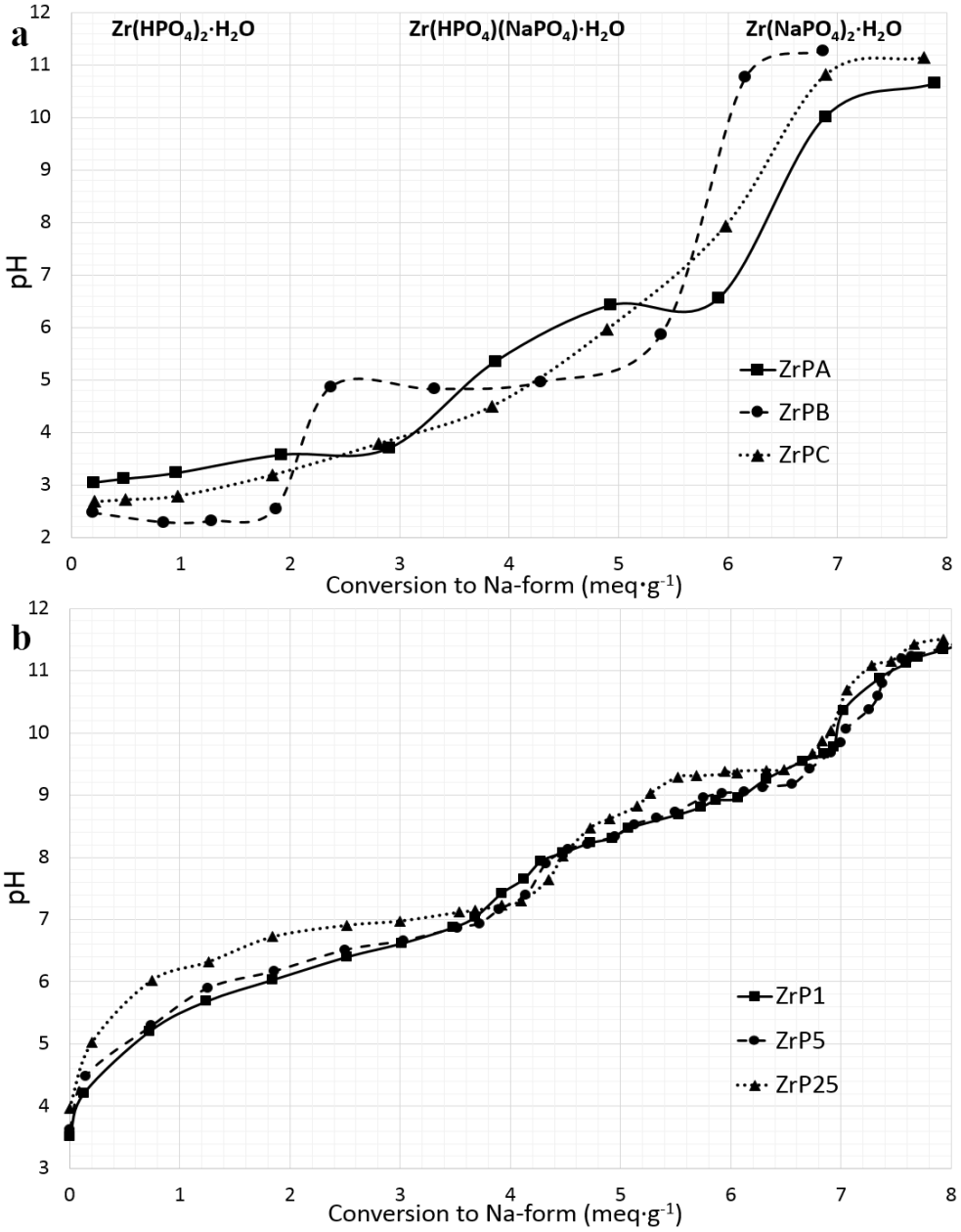

Figure 6. Conversion to Na-form by titration ZrP products with NaOH. (a) The titrations for ZrPA, ZrPB and ZrPC were done in the presence of $NaNO_3$. (b) The titrations for ZrP1, ZrP5 and ZrP25 were done in pure water.

4.1.3 Ion exchange capacity

Capacity in ion exchange can be defined in many ways, in this text we utilize the nomenclature summarized by Friedrich Helfferich in *Ion exchange*.[67] *Maximum capacity*, the number of ionogenic groups per amount of exchanger, is the theoretical capacity that can be calculated from the formula. For pure crystalline α-ZrP, this is 6.64 meq·g^{-1}: 2 moles of exchangeable H^+ per 1 mole of $Zr(HPO_4)_2 \cdot H_2O$, which weighs 301.2 grams. For the products ZrP1, ZrP5 and ZrP25, this capacity per unit weight is a bit higher at 6.8 meq·g^{-1}, since the crystal water content was determined to be less than one (from 0.48 to 0.66 moles per mole), thus molecular weights are less.

Apparent capacity, the number of exchangeable counter ions per amount of exchanger, was determined for all the six synthesized compounds by titration with a strong base (NaOH). The capacity was graphically determined as the sodium conversion at the second equivalence point on the titration curve. For ZrPA and ZrPB, capacities are close to 6.6 meq·g^{-1} and for ZrPC undetermined because of the lack of features of its curve (Fig. 6a). For ZrP1, ZrP5 and ZrP25 however, the capacities were 7.0 meq·g^{-1}, 7.2 meq·g^{-1} and 7.0 meq·g^{-1}, respectively (Fig. 6b). This was explained by the slightly amorphous nature of the products: in the past we have determined values up to 6.97 meq·g^{-1} (maximum theoretical capacity) and 9.2 meq·g^{-1} (apparent capacity) for amorphous ZrP.[46] It was suggested there that higher than maximum capacity can be achieved due to the hydrolysis of the materials in the experimental conditions of the titration.

Perhaps the most interesting capacity for us, the *breakthrough capacity* or *dynamic capacity*, is the capacity determined in column operation for Eu(III) in selected conditions. This was determined for ZrP25 during the column separation work. Two breakthrough experiments were conducted, in equal conditions except for the five-fold difference in the feed rate (Fig. 7). For the faster experiment, with a feed rate of 9 BV·h^{-1} and bed mass 453 mg, the breakthrough capacity was 0.27 meq·g^{-1}. For the slower experiment, 2 BV·h^{-1} and 472 mg, the breakthrough capacity was 0.30 meq·g^{-1}. The attained breakthrough capacity 0.3 meq·g^{-1} is approx. 4% of the apparent capacity of ZrP25, and is a reflection of the real available capacity for Ln(III)'s and An(III)'s in dynamic column applications. It is plausible, that when M^{3+}

enters the interlayer space, it tightens the layers because of its higher charge density, and further M^{3+} ions cannot enter the vicinity of the first one. Thus most Eu and Am would be exchanged to the layer edges and surfaces. Finally, this means that the column capacity could be altered with particle size. However, particles of too small a size would in turn adversely affect the feasibility of real world column use through change in the pressure.

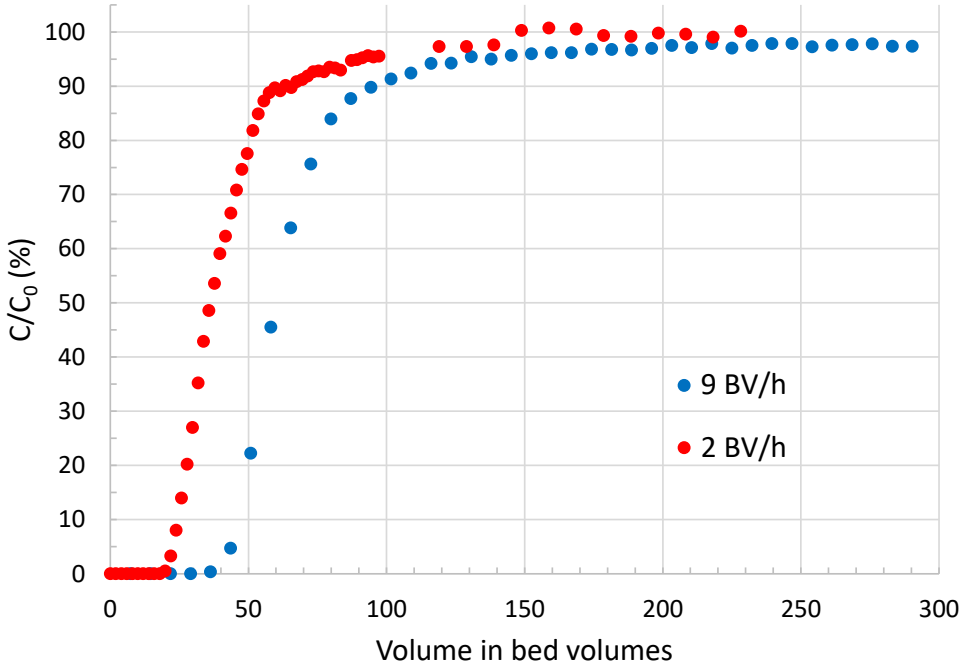

Figure 7. Breakthrough experiments in low pressure columns. Fixed beds of ZrP25, 1.1 mL bed volume in either case, and constant feed of 1 mM solution of Eu(III) in 2 mmol·L^{-1} HNO_3 with 0.1 mol·L^{-1} $NaNO_3$. Feed rate of either 2 or 9 BV·h^{-1}.

4.2 Eu and Am uptake

4.2.1 Distribution, selectivity and metal binding coefficients

As a prerequisite for any column separation experiments, numerous Eu and Am distribution studies were conducted in batch in varying conditions, e.g. as a function of pH or as a function of salts. Whereas most experiments were done with all six products, some were conducted using only ZrP25, which was the selected product for the forthcoming column experiments. Low end of pH scale, from 0 to 3 was always the focus, as the highly acidic streams in the possible applications would require less adjustment there. Conditions suitable for column separation were sought after: a separation factor (SF) as high as possible between Eu and Am. It was quickly noted that ZrP always favours Eu in our experimental conditions. Thus, optimal separation conditions would be those where Eu uptake would be as high as possible, while Am the opposite.

The distribution coefficients (K_d, Equation 6) were determined in pH 0 to 3 nitric acid with 0.1 mol·L^{-1} $NaNO_3$ for all 6 products (Fig. 8). For any given product, the K_d for Eu is around 5 to 100 times higher than for Am in a given pH, thus the SF (the ratio K_d(Eu) : K_d(Am)) varies from 5 to 100. The plot of log K_d versus pH_{eq} is expected to be linear with a slope of 3 for purely H^+ to M^{3+} ion exchange (see Equation 5). The reported slopes are from 2.3 to 2.7 for ZrPA, ZrPB and ZrPC, with the exception of 3.4 for Eu and ZrPA, and from 2.6 to 3.0 for ZrP1, ZrP5 and ZrP25. With very high K_d, the linearity is lost as a very high K_d is underestimated. Some extremely high K_d (> 1 000 000) data points are omitted, as the measured sample radioactivity gets equal with the background even with long measurement times, resulting in extreme uncertainty.

The case of slope 3.4 remains unexplained though the value was calculated based on only three data points. Lower than 3 slopes are explained with competing sorption mechanisms to the expected H^+ to M^{3+} ion exchange, e.g. the exchange of H^+ for $M(NO_3)^{2+}$. Based on species calculations with PHREEQC code, in pH 0 to 3 nitric acid, 32 to 60% of Am and 12 to 31% of Eu are present as $M(NO_3)^{2+}$. In our experimental conditions, and in contact with air, no other species (such as carbonates or hydroxides) are present, only M^{3+} and $M(NO_3)^{2+}$. The two to three-fold difference in speciation definitely plays an important role in the separation

properties. This is supported by the fact that Am, which has less retention, i.e. the lower K_d, has larger fraction as the large divalent ion.

In summary, the order of preference for ZrP, Eu over Am, can be explained with a combination of the following three elements:

i) The Pearson's Hard-Soft-Acid-Base (HSAB) principle states that a hard base (phosphate) binds a harder acid (Eu) stronger.

ii) In our experimental conditions in the solution, only the species M^{3+} and $M(NO_3)^{2+}$ are present for M = Eu, Am. Considerably larger fraction of Am than Eu is present as $M(NO_3)^{2+}$, which is exchanged less than M^{3+} to the solid phase, if at all.

iii) The narrow structure acts as an ion sieve and prefers the smaller Eu with the higher charge density.

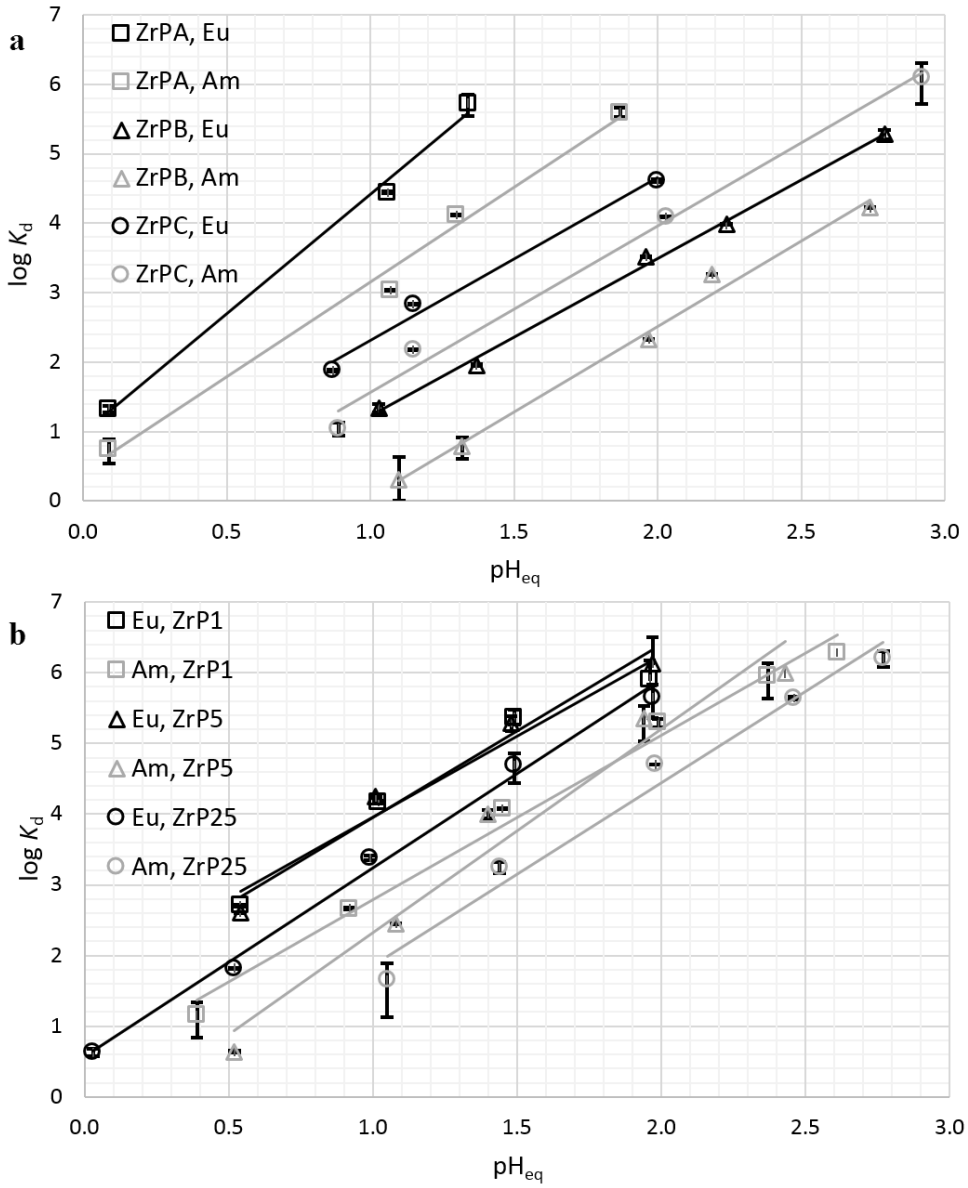

Figure 8. Distribution coefficients (K_d) for Eu and Am sorption on zirconium phosphates (a) ZrPA, ZrPB and ZrPC, (b) ZrP1, ZrP5 and ZrP25, in 0.001 mol·L^{-1} to 1 mol·L^{-1} HNO_3 with 0.1 mol·L^{-1} $NaNO_3$.

For ZrP25, the effect of mono- and divalent cations on Eu uptake was studied using 0.1 and 0.01 mol·L^{-1} salts $NaNO_3$, NaCl and $SrCl_2$. Between the Na salts, the anion did not play any significant role (Table 3). Between Na and Sr, the increase in Na

concentration had a positive effect on Eu uptake, whereas for Sr it did not. This was further investigated using $NaNO_3$, from 0.001 mol·L^{-1} to 4 mol·L^{-1}. (Fig. 9) The trend is clear as K_d reliably increases from 0.001 mol·L^{-1} to 0.2 mol·L^{-1} in comparable pH_{eq}. After the salt concentration is further increased, the K_d starts to decrease, at first most likely due to only the lower pH_{eq} in the experiment, and finally due to the sheer overwhelming of Na concentration versus carrier free trace Eu concentration: 10^{11}-fold difference.

Table 3. Comparison of the effect of Na(I) and Sr(II) concentration on Eu(III) distribution coefficient in nitric acid for ZrP25.

Salt	Concentration mol·L^{-1}	K_d Eu(III)	pHeq
NaCl	0.1	4135	1.05
	0.01	2525	1.06
$SrCl_2$	0.1	2452	1.01
	0.01	2491	1.03
$NaNO_3$	0.1	4204	1.00
	0.01	2999	1.02

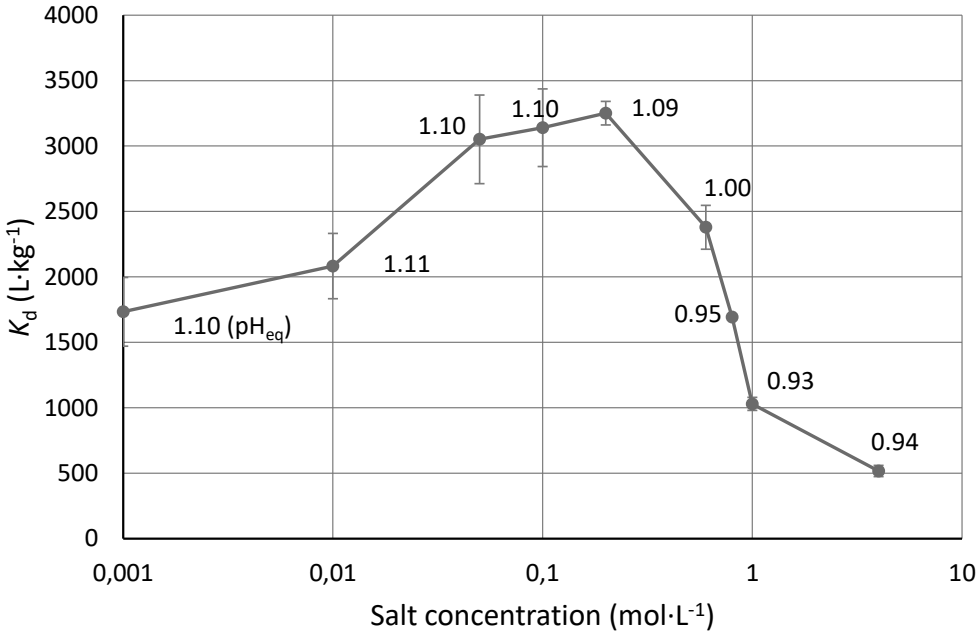

Figure 9. Distribution coefficient for trace Eu as a function of $NaNO_3$ concentration, from 0.001 mol·L^{-1} to 4 mol·L^{-1}, for ZrP25. Values next to the data points are the measured equilibrium pH values.

Kinetics experiments were conducted on ZrP25 for both trace Eu and Am, both together in the same solution (Fig. 10) and separately (Fig. 11). No significant differences between the two experiments were noted. Eu uptake reaches equilibrium after 24 hours. Am uptake reaches its brief maximum after two hours, after which it starts to decrease. The decrease is not due to Eu-Am competition, as the phenomenon is seen also in the separate solutions experiment. Possibility of self-milling of particles to a sub-filter size was discussed, but ruled out for three reasons: i) for Eu, the uptake rises steadily before and after the same two hours, ii) stability of both highly crystalline and highly amorphous ZrP has been proven earlier in similar kinetics study for Nd and Dy,[44,46] iii) more demanding filtration was applied with no difference in the outcome (Fig. 11). What is then left to account for the behaviour that is seen for Am but not for Eu? The effect of the third cation present, in abundance, Na. As seen for Eu in the previous experiments, the used concentration of Na (0.1 mol·L^{-1}) only increases Eu uptake in three-day batch

experiments (Tables 3 and 5, Fig. 9), meaning that ZrP greatly favours Eu over Na regardless of the great difference in the concentrations. The evidence suggest that this is not the case for Am. Am is first taken up by the exchanger with fast kinetics, but after two hours, when more and more Na is exchanged due to its slower kinetics, Am is pushed out due to the huge difference in the concentrations.

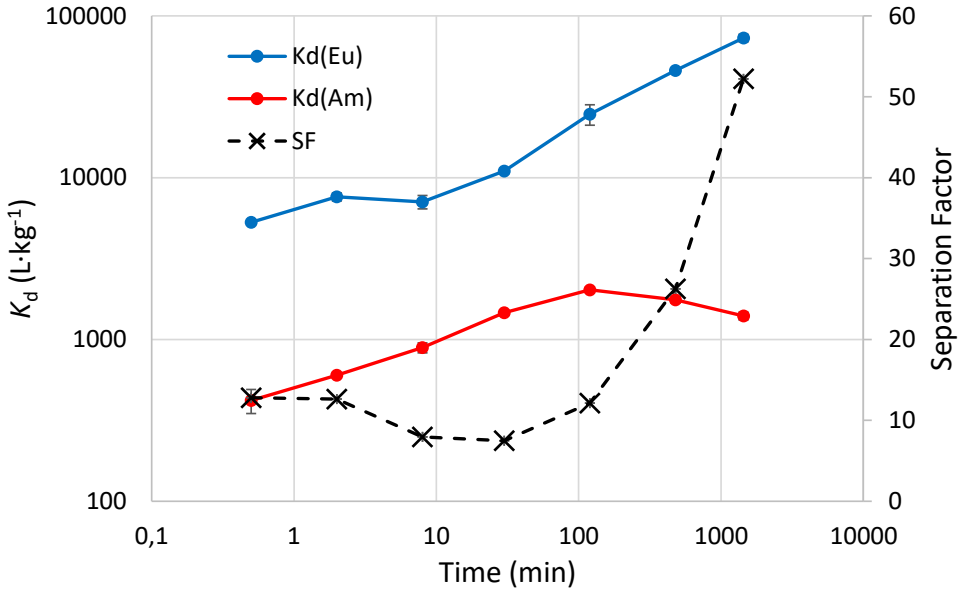

Figure 10. The distribution coefficients for ZrP for Eu(III) and Am(III) in a binary solution, nitric acid (pH 1.5) with 0.1 mol·L^{-1} $NaNO_3$ as a function of equilibrating time, up to 24 hours. The separation factor (SF) is calculated as K_d(Eu): K_d(Am).

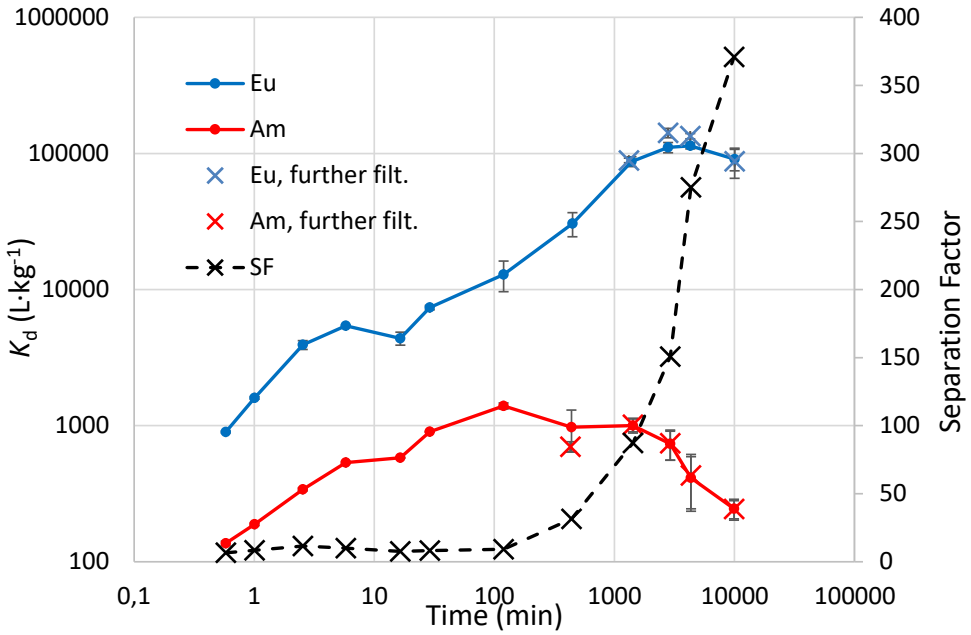

Figure 11. The distribution coefficients for ZrP for Eu(III) and Am(III) in separate solutions of nitric acid (pH 1.5) containing 0.1 mol·L^{-1} $NaNO_3$ as a function of equilibrating time, up to 1 week. The separation factor (SF) is calculated as K_d(Eu): K_d(Am).

From the log K_d versus pH_{eq} plots, the selectivity coefficients (Table 4) $k_{M/H}$ were determined based on Equation 5. It is simplified in our case (M = Eu or Am, $Z_M = 3$) that

$$\log k_{M/H} = IC - 3 \times \log Q,$$

where Q is the maximum capacity of the exchanger, and IC is the intercept. The selectivity coefficient is a parameter that gives the difference in affinities of M over H of the exchanger. Further, the metal binding coefficients (Table 4) were calculated from the selectivity coefficients and the acid dissociation constants (pK_{a1}) based on Equation 20. Metal binding coefficient is a parameter that gives the raw affinity of an exchanger for an ion.

For the series of ZrP1, ZrP5 and ZrP25, small differences between ZrP1 and ZrP5 were noted, whereas ZrP25 is more unique. Even though ZrP25 has a lower

selectivity coefficient for both Eu/H and Am/H than ZrP1 and ZRP5, the metal binding is stronger. It is the least acidic as its pK_{a1} is highest. The differences in $k_{M/H}$ and k_M between Eu and Am for ZrP25 are approx. 25-fold, whereas for ZrP1, they are only ten-fold. For ZrP5, they are even 50-fold, meaning it has the highest selectivity differences between Eu and Am. As reported in paper **II**, it has the highest SF in pH 0.5 and 1.0, but not in pH 1.5 or higher. There, ZrP25 has the highest.

In the case of the series ZrPA, ZrPB and ZrPC, the metal binding coefficients were calculated, but incorrectly from the smaller-than-true *apparent* pK_a. They can still be compared amongst each other, though. In this case, the most amorphous ZrPA had both the largest selectivity coefficients and the highest apparent metal binding. The differences between Eu and Am for ZrPA were the smallest of the three however, meaning that its separation capabilities are not that good.

Table 4. Selectivity coefficients and metal binding coefficients for the zirconium phosphates ZrP1, ZrP5, ZrP25, ZrPA, ZrPB and ZrPC.

		ZrP1	ZrP5	ZrP25	ZrPA	ZrPB	ZrPC
log $k_{M/H}$	Eu	-1.305	-1.377	-2.195	-1.48	-3.51	-2.49
	Am	-2.320	-3.103	-3.559	-2.04	-4.87	-3.29
log k_M	Eu	17.055	17.523	18.445	9.02*	3.39*	6.81*
	Am	16.040	15.797	17.081	8.46*	2.03*	6.01*

*The metal binding coefficients for ZrPA, ZrPB and ZrPC were calculated based on *apparent* pK_a and are not comparable with the others.

4.2.2 Competitive uptake

The distribution studies described in chapter 4.2.1 were always made in separate solutions for Eu and Am. To account for possible competition, Am distribution was studied as a function of Eu molarity, from 1:40 Eu to Am molar ratio to 10 000:1 (Table 5). When Eu is present in lesser concentration, Am uptake is at its highest. Am uptake stays in similar or even higher levels than when Am distribution is studied on its own (0:1), until Eu concentration is increased to more than ten-fold

levels. After this, minor and decreasing portion of Am is taken by the exchanger as Eu levels increase from 100- to 10 000-fold in molar concentration. Thus, the competition drives separation even in the levels where practical capacity is not reached.

Table 5. The distribution coefficients (K_d) and the separation factors (SF, K_d(Eu) : K_d(Am)) for Eu and Am at selected Eu to Am molar ratios. ZrP25 in nitric acid containing 0.1 mol·L^{-1} sodium nitrate (pH_{eq} = 1.5).

K_d(Eu), L·kg^{-1}	K_d(Am), L·kg^{-1}	SF	Eu : Am
	730		0 : 1
140 000	1 300	102	1 : 39
140 000	1 700	83	1 : 16
110 000	860	125	1 : 1.2
	760		10 : 1
	65		100 : 1
	49		500 : 1
	40		1000 : 1
	31		10000 : 1

Effect of pH on uptake in binary solutions was investigated with and without added sodium nitrate (Table 6). In contrast to the SF 100 achieved in separate solutions for any of the six products, up to 400 SF was achieved in binary solutions, in pH 1 with a new batch of ZrP25 that was synthesized for paper **III**. This seemingly high improvement can be accounted by *i*) the very low K_d of Am in low pH: even a small change in the small denominator has great effect on the ratio, and *ii*) possibly the effect of Eu on Am uptake. Since both analytes are in trace, with equal tracer radioactivity and thus a 1:32 molar ratio, the latter (*ii*) should be ruled out based on the findings reported in Table 5.

In pH 1.5, an increase in K_d for also Am can be seen from the samples with no $NaNO_3$ to the ones with added $NaNO_3$, controversially to what was discussed earlier. However, this can be explained by the ten-fold increase in Eu in the exchanger in the binary samples: K_d(Am) is increased due to the positive effect of Eu uptake that overwhelms the negative effect of Na uptake. But on its own, K_d(Am) would decrease due to the presence of Na, as seen earlier.

It then becomes plausible, that could the Eu-Am separation be enhanced by the addition of greater levels of salt(s)? Eu uptake would not be hindered as much as Am, and thus the SF could be driven up. This idea was not explored during the thesis work, but should definitely be considered for future studies.

Table 6. The distribution coefficients (K_d) and the separation factors (SF, K_d(Eu) : K_d(Am)) for trace Eu and Am in binary solution. ZrP25 in nitric acid with and without sodium nitrate.

With 0.1 mol·L^{-1} $NaNO_3$				Without $NaNO_3$			
pH_{eq}	K_d(Eu)	K_d(Am)	SF	pH_{eq}	K_d(Eu)	K_d(Am)	SF
0.49	14	18	0.77	0.49	46	13	3.6
0.99	2800	6.9	410	1.01	1900	14	130
1.48	140000	1300	110	1.50	16000	350	44
2.01	high	19000	n/a	2.00	high	16000	n/a

4.3 Column separation of Eu and Am

ZrP25 was the product selected for final column separation experiments for the two major reasons: *i*) it was established that it had good separation capabilities in the region of pH 1 to 1.5 based on all preliminary experiments, *ii*) it had a clear, most crystalline structure and, possibly for that reason, *iii*) it was readily usable in dynamic column operation. Throughout the years, other ZrP products were tested in column operation with varying success, the most common problem being a build-up of high pressure perhaps due to the instability of the particles in dynamic environment. To overcome this, at one time the product ZrPB was bound to silica, but such means had too adverse an effect on the separation capability. Such problems were never seen for ZrP25, it was ready for column use as such.

Two types of column experiments were conducted. In the first type (Chapter 4.3.1), the column was loaded with both Eu and Am in such conditions where the K_d was very high for both elements, to make sure they would accumulate together on the very top of the column in a narrow volume. The elution conditions were then selected as to selectively elute the less-bound Am, thus separating it from Eu. The second type of experiment (Chapter 4.3.2) was the continuous feed experiment,

where a constant feed of Eu and Am in equimolar concentration was pumped through the column, and the elute concentrations were monitored in small fractions until the levels reached the feed levels.

4.3.1 Load-elution column experiments

Several load-elution type column experiments were conducted over the years, the latest and most optimized of which is reported here. The product ZrP25 was used in low-pressure column environment, with feed rates of 8 to 16 $BV \cdot h^{-1}$ (Fig. 12). During the loading of the column in high K_d conditions, no leakage of either analyte was detected.

Region I: separation. From the start of the elution, 0.18 $mol \cdot L^{-1}$ HNO_3 with 0.1 $mol \cdot L^{-1}$ $NaNO_3$ was supplied with the rate 8 $BV \cdot h^{-1}$. The majority of the loaded Am eluted before a total of 130 BV's. Only miniscule amounts of Am were detected afterwards. Europium did not reach detectable amounts before 40 BV's, but reached significant levels soon after.

Region II: expedited elution. To test if more Am could be recovered with stronger acid, 1 $mol \cdot L^{-1}$ HNO_3 with 0.1 $mol \cdot L^{-1}$ $NaNO_3$ was supplied with the rate 16 $BV \cdot h^{-1}$. No additional Am was eluted, but the elution of Eu was enhanced.

Region III: additional ideas. A high concentration of NH_4^+ was supplied to see whether the layered structure could be opened up and Am elution improved. First, 0.002 $mol \cdot L^{-1}$ HNO_3 with 0.1 $mol \cdot L^{-1}$ $NaNO_3$ and 2 $mol \cdot L^{-1}$ NH_4NO_3 was fed with the rate 16 $BV \cdot h^{-1}$ and last, 1 $mol \cdot L^{-1}$ HNO_3 with 0.1 $mol \cdot L^{-1}$ $NaNO_3$ and 1 $mol \cdot L^{-1}$ NH_4NO_3 with the same rate. No additional Am was eluted.

A total of 93% of the loaded Am was eluted during the whole experiment and the rest could not be recovered even in stronger acid. This 93% was hence named *the available fraction of Am*. This suggests that some other mechanisms play a small role in the sorption in addition to ion exchange. These mechanisms could also explain the lower than 3 slopes discussed in Chapter 4.2.1.

82% of the available Am was eluted and separated from Eu with 99.999% molar purity in the first combined 39 BV's. Alternatively, 95% of the available Am could be separated with 99.7% molar purity in the first combined 130 BV's.

Most overlap between Eu and Am is in the region from 40 to 130 BV's. In a following experiment, the corresponding fractions were supplied to another fresh column of ZrP25 in the same amount, where a similar load-elution type experiment was conducted. In summary, if the purest of fractions from the first experiment were to be combined with the purified fractions from the second experiment, 93% of the available Am could be separated from Eu with 99.86% molar purity. This result averages both the recoveries and the purities from the two one-column example calculations in the previous paragraph: a higher recovery is combined with higher purity. However, the experiment is made twice as complex, and more importantly uses twice as much exchanger. It is plausible that a less pure Am stream (e.g. ~99%) is pure enough for an application such as transmutation, and then parameters such as the recovery % would be the deciding factors in process design, but such discussion is out of scope for this text.

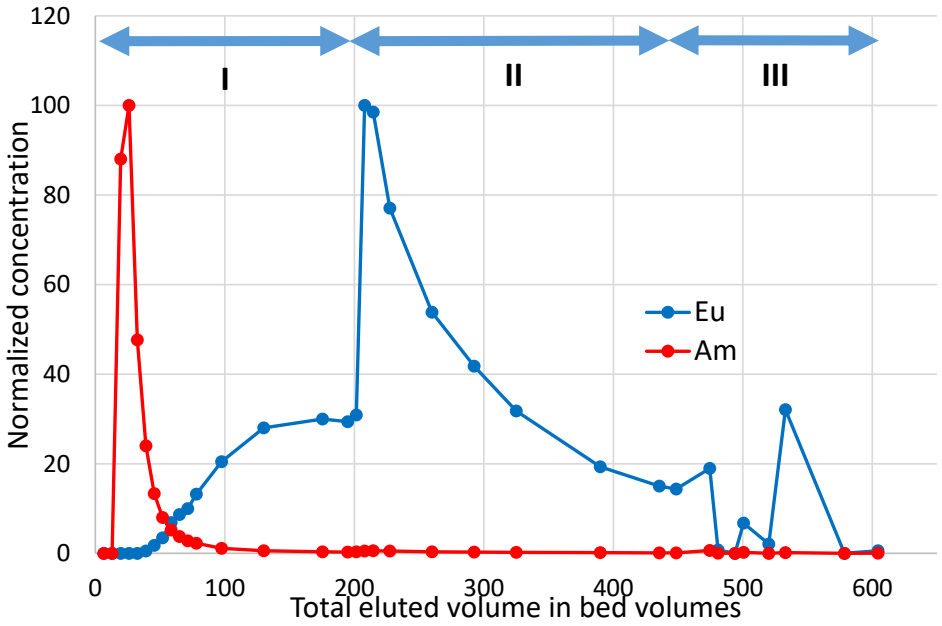

Figure 12. The normalized concentration of Eu and Am in the eluate, measured periodically from the fractionated eluate, as a function of the total volume.

4.3.2 Continuous feed column experiment

The column separation of Eu and Am from continuous feed was investigated with ZrP25 (Fig. 13). In the feed, Eu and Am were in equimolar concentration (1 nmol·L^{-1}). Based on all the previous work, such conditions were selected where Am would have small to no retention, and at the same time, Eu would have as high as possible. The selected feed was 0.1 mol·L^{-1} HNO_3 with 0.1 mol·L^{-1} $NaNO_3$, where K_d's were determined together in a binary solution: 2800 L·kg^{-1} and 7 L·kg^{-1} for Eu and Am, respectively (Table 6).

As soon as a total of 50 BV's were eluted, Am had reached the feed levels. For Eu, it took 450 BV's. In summary, up to 330 L·kg^{-1} of the equimolar Eu-Am mixture was eluted with molar Am purity staying above 99.5% in the total cumulative volume of eluate. Alternatively, up to 630 L·kg^{-1} could be treated with >95% molar purity, or up to 800 L·kg^{-1} with >90%. The eluate levels for Am higher than 100% could be explained by the brief sorption of Am in the most readily available ion exchange sites, followed by replacement by Eu. Later, the eluting Am settles at 100% of feed concentration levels.

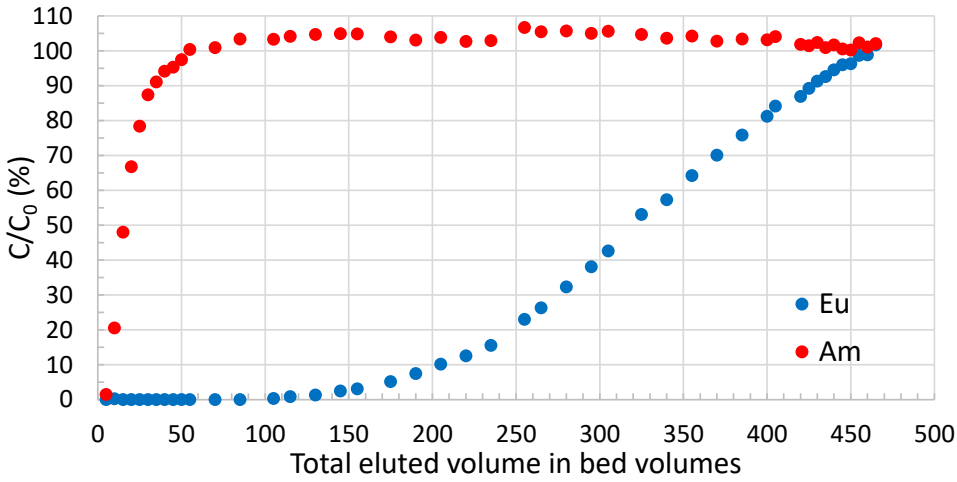

Figure 13. Continuous feed column experiment with ZrP25 and equimolar (1 nmol·L^{-1}) binary solution of Eu and Am in 0.1 mol·L^{-1} HNO3 and 0.1 mol·L^{-1} NaNO3. Bed volume 1.0 mL, feed rate 5.0 BV·h^{-1}, and bed mass 443 mg.

5 Conclusions

Summary of key findings:

- Systematic studies were conducted with the six synthesized products
    - The acidity and therefore the ion exchange properties of ZrP can be modified through small changes in the synthesis procedure
    - ZrP favours Eu over Am in nitric acid media, with separation factors commonly from 5 to 100, up to 400
    - Such order of selectivity is preferable in regard to P&T strategies: the radiotoxic Am could be separated for transmutation, while Eu could be kept in the solid exchanger phase, suitable for final disposal
- Advanced experiments were conducted with a selected product, ZrP25
    - ZrP is extremely selective for Eu(III) over Na(I) or Sr(II), even when Eu is vastly overnumbered, e.g. 10^{11}-fold
    - Am uptake is debatably hindered by Na
    - Am uptake is increased slightly in the presence of dilute Eu, but is hindered by excess (>ten-fold) concentration of Eu
    - This enhances the separation if Eu (perhaps other lanthanides) are in excess in an application
    - Majority of Am could be recovered from the ZrP columns, but not all, suggesting a minor mechanism in addition to plain ion exchange
    - In the selective elution experiment, 82% of the recoverable Am (= 93% of total Am) were separated from Eu with >99.999% molar purity. Alternatively, 95% with >99.7% molar purity.
    - In the constant feed experiment, up to 330 $L \cdot kg^{-1}$ of an equimolar Eu-Am mixture was treated with Am molar purity >99.5% in the total eluate. Alternatively, up to 630 $L \cdot kg^{-1}$ with >95%.

Although the bulk structure shows only equivalent POH groups in α-ZrP, from the titration results it was concluded that even the bulk material acts as if it were a molecular diprotic acid, corresponding to its chemical structure $Zr(HPO_4)_2 \cdot H_2O$. After the first half of the available hydrogens are exchanged (pK_{a1}), the other half

becomes less accessible. For three of the materials under study, the *true* pK_{a1} determined in pure water were between 6 and 7. For another three of the materials, the *apparent* pK_{a1} values in experimental conditions, with Na present, were between 2 and 4. It was concluded that the acidity and thus the ion exchange properties can be altered even with minimal changes in the synthesis procedure. The first obvious application for this would be to reach a specific level of uptake in different pH conditions: the more acidic variant of ZrP can be used in very low pH, and the less acidic variant in higher pH.

The apparent ion exchange capacities were determined to be close to the theoretical 6.64 meq·g^{-1} value for the highly crystalline materials, and higher (from 7.0 to 7.2 meq·g^{-1}) for the semi-crystalline materials. In column conditions, for Eu, the breakthrough capacity was determined to be 0.3 meq·g^{-1} which is approx. 4% of the apparent capacity. This highlights the usual case that in dynamic conditions for M^{3+}, only the most accessible exchange sites are available. It was discussed that most of the Eu and Am is exchanged to the layer edges and surfaces. This means that the column's breakthrough capacity can be increased with a smaller particle size. However, this in turn affects the feasibility of a real-world column use through an increase in the pressure. For highly radioactive applications, where the use of column material is also limited by an upper limit in the retained radioactivity for the reasons of safety and material stability, a reduction of the capacity in such a simple way as increasing the particle size can be advantageous.

The roots of SNF processing are in the ion exchange. Throughout decades, the focus quickly shifted towards solvent extraction and a spectrum of alternative technologies. Through my thesis work, I have learned and also hope to have shown, that ion exchange can still excel in very specific jobs. Whereas the well-established solvent extraction-based separation processes can handle the reprocessing relatively fine, I believe that ion exchange could have a supportive role in their shortcomings. World will never run out of new ion exchangers, whether cheap, simple, inorganic or green – or perhaps elaborate surface grafted hybrid ones. Ion exchangers can be engineered to target the most difficult problems, and by their nature are well suited for online column use in industrial processes.

Literature

1. OECD/NEA, Accelerator-driven Systems (ADS) and Fast Reactors (FR) in Advanced Nuclear Fuel Cycles (2002).
2. IAEA, Implications of Partitioning and Transmutation in Radioactive Waste Management, Technical report series, No. 435 (2004).
3. OECD, National Inventories and Management Strategies for Spent Nuclear Fuel and Radioactive Waste, NEA No. 7323 (2016).
4. Häkkinen, S., Wiikinkoski, E.: Kehittyneet polttoainekierrot maailmalla, VTT Technical Research Centre of Finland, No. VTT-R-00255-19 (2019).
5. Mohan, M. P. R., Aggarwal, V.: Spent fuel management in India. Journal of Risk Research 12, 955 (2009).
6. Zhou, Y.: China's spent nuclear fuel management: Current practices and future strategies. Energy Policy 39, 4360 (2011).
7. OECD, State-of-the-Art Report on the Progress of Nuclear Fuel Cycle Chemistry (2018).
8. Choppin, G. R., Liljenzin, J.-O., Rydberg, J. A. N., in *Radiochemistry and Nuclear Chemistry (Third Edition)*, edited by Gregory R. Choppin, Jan-Olov Liljenzin, J. A. N. Rydberg (Butterworth-Heinemann, Woburn, 2002), pp. 583.
9. Bourg, S., Hill, C., Caravaca, C., Rhodes, C., Ekberg, C., Taylor, R., Geist, A., Modolo, G., Cassayre, L., Malmbeck, R., Harrison, M., de Angelis, G., Espartero, A., Bouvet, S., Ouvrier, N.: ACSEPT—Partitioning technologies and actinide science: Towards pilot facilities in Europe. Nuclear Engineering and Design 241, 3427 (2011).
10. Mathur, J. N., Murali, M. S., Nash, K. L.: Actinide Partitioning—A Review. Solvent Extraction and Ion Exchange 19, 357 (2001).
11. Nash, K. L., in *Handbook on the Physics and Chemistry of Rare Earths* (Elsevier, 1994), Vol. 18, pp. 197.
12. Paiva, A. P., Malik, P.: Recent advances on the chemistry of solvent extraction applied to the reprocessing of spent nuclear fuels and radioactive wastes. Journal of Radioanalytical and Nuclear Chemistry 261, 485 (2004).
13. Ensor, D. D., Jarvinen, G. D., Smith, B. F.: The Use Of Soft Donor Ligands, 4-Benzoyl-2,4-Dihydro-5-Methyl-2-Phenyl-3h-Pyrazol-3-Thione And 4,7-Diphenyl-uo-Phenanthroline, For Improved Separation Of Trivalent Americium And Europium. Solvent Extraction and Ion Exchange 6, 439 (1988).
14. Nash, K. L.: The Chemistry of TALSPEAK: A Review of the Science. Solvent Extraction and Ion Exchange 33, 1 (2015).
15. Ozawa, M., Sano, Y., Tanaka, Y.: CMPO-TRUEX Process and its Application in the Separation of Actinides from High-Level Liquid Wastes. Mineral Processing and Extractive Metallurgy Review 21, 249 (2000).
16. Drain, F., Emin, J. L., Vinoche, R., Baron, P., presented at the WM'08: Waste Management Symposium 2008 - HLW, TRU, LLW/ILW, Mixed, Hazardous Wastes and Environmental Management - Phoenix Rising: Moving Forward in Waste Management, United States, 2008 (unpublished).
17. Modolo, G., Vijgen, H., Serrano-Purroy, D., Christiansen, B., Malmbeck, R., Sorel, C., Baron, P.: DIAMEX Counter-Current Extraction Process for Recovery of Trivalent Actinides from Simulated High Active Concentrate. Separation Science and Technology 42, 439 (2007).
18. Heres, X., Baron, P., Hill, C., Ameil, E., Martinez, I., Rivalier, P., presented at the Atalante 2008: Nuclear fuel cycle for a sustainable future, France, 2008 (unpublished).

19. Schultz, W. W.: Macroreticular Ion Exchange Resin Cleanup of Purex Process TBP Solvent, Atlantic Richfield Hanford Company, Richland, Washington, (1970).
20. Rahman, M. K.: Clean up of the purex process TBP solvent by macroreticular ion exchange resin. Radiochimica Acta 22, 53 (1975).
21. Navratil, J. D.: Ion Exchange Technology in Spent Fuel Reprocessing. Journal of Nuclear Science and Technology 26, 735 (1989).
22. Xu, L., Xiao, Y., van Sandwijk, A., Xu, Q., Yang, Y., presented at the Energy Materials 2014, Cham, 2016 (unpublished).
23. Lehto, J., Koivula, R., Leinonen, H., Tusa, E., Harjula, R.: Removal of Radionuclides from Fukushima Daiichi Waste Effluents. Separation & Purification Reviews 48, 122 (2019).
24. Lehto, J., Hou, X., *Chemistry and Analysis of Radionuclides: Laboratory Techniques and Methodology*. (Wiley-VCH Verlag GmbH & Co. KGaA, 2010).
25. Shannon, R.: Revised effective ionic radii and systematic studies of interatomic distances in halides and chalcogenides. Acta Crystallographica Section A 32, 751 (1976).
26. Pica, M.: Zirconium phosphate catalysts in the XXI century: State of the art from 2010 to date. Catalysts 7, (2017).
27. Clearfield, A., Thakur, D. S.: Zirconium and titanium phosphates as catalysts: a review. Applied Catalysis 26, 1 (1986).
28. Ferlin, F., Cappelletti, M., Vivani, R., Pica, M., Piermatti, O., Vaccaro, L.: Au@zirconium-phosphonate nanoparticles as an effective catalytic system for the chemoselective and switchable reduction of nitroarenes. Green Chemistry 21, 614 (2019).
29. Pica, M., Calzuola, S., Donnadio, A., Gentili, L. P., Nocchetti, M., Casciola, M.: De-Ethylation and Cleavage of Rhodamine B by a Zirconium Phosphate/Silver Bromide Composite Photocatalyst. Catalysts 9, (2018).
30. Pica, M., Nocchetti, M., Ridolfi, B., Donnadio, A., Costantino, F., Gentili, P. L., Casciola, M.: Nanosized zirconium phosphate/AgCl composite materials: a new synergy for efficient photocatalytic degradation of organic dye pollutants. Journal of Materials Chemistry A 3, 5525 (2015).
31. Vaivars, G., Mokrani, T., Hendricks, N., Linkov, V.: Inorganic membranes based on zirconium phosphate for fuel cells. Journal of Solid State Electrochemistry 8, 882 (2004).
32. Bauer, F., Willert-Porada, M.: Characterisation of zirconium and titanium phosphates and direct methanol fuel cell (DMFC) performance of functionally graded Nafion(R) composite membranes prepared out of them. Journal of Power Sources 145, 101 (2005).
33. Casciola, M.: From layered zirconium phosphates and phosphonates to nanofillers for ionomeric membranes. Solid State Ionics 336, 1 (2019).
34. Alberti, G., Casciola, M., Pica, M., Di Cesare, G.: Preparation of Nano-Structured Polymeric Proton Conducting Membranes for Use in Fuel Cells. Annals of the New York Academy of Sciences 984, 208 (2003).
35. Brunet, E., Alhendawi, H. M. H., Cerro, C., de la Mata, M. J., Juanes, O., Rodríguez-Ubis, J. C.: Hydrogen Storage in a Highly Porous Solid Derived from γ-Zirconium Phosphate. Angewandte Chemie International Edition 45, 6918 (2006).
36. Colón, J. L., Casañas, B., in *Tailored Organic-Inorganic Materials*, edited by E. Brunet, J. L. Colón, A. Clearfield (John Wiley & Sons, Inc, Hoboken, NJ, 2015).
37. Saxena, V., Diaz, A., Clearfield, A., Batteas, J. D., Hussain, M. D.: Zirconium phosphate nanoplatelets: a biocompatible nanomaterial for drug delivery to cancer. Nanoscale 5, 2328 (2013).
38. Mosby, B. M., Diaz, A., Clearfield, A.: Surface modification of layered zirconium phosphates: a novel pathway to multifunctional materials. Dalton Transactions 43, 10328 (2014).
39. Clearfield, A.: Inorganic ion exchangers with layered structures. Ann. Rev. Mater. Sci. 14, 205 (1984).

40. Kullberg, L., Clearfield, A.: Mechanism of ion exchange in zirconium phosphates. 32. Thermodynamics of alkali metal ion exchange on crystalline α-ZrP. Journal of Physical Chemistry 85, 1585 (1981).
41. Alberti, G., Costantino, U.: Recent progress in the field of synthetic inorganic exchangers having a layered or fibrous structure. Journal of Chromatography 102, 5 (1974).
42. Komarneni, S., Roy, R.: Use of γ-zirconium phosphate for Cs removal from radioactive waste. Nature 299, 707 (1982).
43. Möller, T., Bestaoui, N., Wierzbicki, M., Adams, T., Clearfield, A.: Separation of lanthanum, hafnium, barium and radiotracers yttrium-88 and barium-133 using crystalline zirconium phosphate and phosphonate compounds as prospective materials for a Ra-223 radioisotope generator. Applied Radiation and Isotopes 69, 947 (2011).
44. Xu, J., Wiikinkoski, E., Koivula, R., Zhang, W., Ebin, B., Harjula, R.: HF-Free Synthesis of α-Zirconium Phosphate and Its Use as Ion Exchanger for Separation of Nd(III) and Dy(III) from a Ternary Co–Nd–Dy System. Journal of Sustainable Metallurgy 3, 646 (2017).
45. Xu, J., Virolainen, S., Zhang, W., Kuva, J., Sainio, T., Koivula, R.: Polyacrylonitrile-encapsulated amorphous zirconium phosphate composite adsorbent for Co, Nd and Dy separations. Chemical Engineering Journal 351, 832 (2018).
46. Xu, J., Koivula, R., Zhang, W., Wiikinkoski, E., Hietala, S., Harjula, R.: Separation of cobalt, neodymium and dysprosium using amorphous zirconium phosphate. Hydrometallurgy 175, 170 (2018).
47. Mimura, H., Akiba, K.: Adsorption behavior of americium on granulated zirconium phosphate. Journal of Nuclear Science and Technology 32, 819 (1995).
48. Mimura, H., Akiba, K.: Adsorption properties of europium on granulated α-zirconium phosphate. Journal of Nuclear Science and Technology 33, 592 (1996).
49. Wiikinkoski, E. W., Harjula, R. O., Lehto, J. K., Kemell, M. L., Koivula, R. T., in *Radiochimica Acta* (2017), Vol. 105, p. 1033.
50. Wiikinkoski, E. W., Xu, J., Zhang, W., Hietala, S., Koivula, R. T.: Modification of α-Zirconium Phosphate Synthesis – Effects of Crystallinity and Acidity on Eu(III) and Am(III) Ion Exchange. 3, 9583 (2018).
51. Clearfield, A., Stynes, J. A.: The preparation of crystalline zirconium phosphate and some observations on its ion exchange behaviour. Journal of Inorganic and Nuclear Chemistry 26, 117 (1964).
52. Clearfield, A., Blessing, R. H., Stynes, J. A.: New crystalline phases of zirconium phosphate possessing ion-exchange properties. Journal of Inorganic and Nuclear Chemistry 30, 2249 (1968).
53. Poojary, D. M., Shpeizer, B., Clearfield, A.: X-Ray powder structure and Rietveld refinement of γ-zirconium phosphate, $Zr(PO_4)(H_2PO_4)\cdot 2H_2O$. Journal of the Chemical Society, Dalton Transactions 111 (1995).
54. Krogh Andersen, A. M., Norby, P., Hanson, J. C., Vogt, T.: Preparation and Characterization of a New 3-Dimensional Zirconium Hydrogen Phosphate, τ-$Zr(HPO_4)_2$. Determination of the Complete Crystal Structure Combining Synchrotron X-ray Single-Crystal Diffraction and Neutron Powder Diffraction. Inorganic Chemistry 37, 876 (1998).
55. Pica, M., Vivani, R., Donnadio, A., Troni, E., Fop, S., Casciola, M.: Small is Beautiful: The Unusual Transformation of Nanocrystalline Layered α-Zirconium Phosphate into a New 3D Structure. Inorganic Chemistry 54, 9146 (2015).
56. Kijima, T.: Direct Preparation of θ-Zirconium Phosphate. Bulletin of the Chemical Society of Japan 55, 3031 (1982).
57. Alberti, G., Costantino, U., Gill, J. S.: Crystalline insoluble acid salts of tetravalent metals—XXIII: Preparation and main ion exchange properties of highly hydrated zirconium bis

monohydrogen orthophosphates. Journal of Inorganic and Nuclear Chemistry 38, 1733 (1976).
58. Clearfield, A., Duax, W. L., Medina, A. S., Smith, G. D., Thomas, J. R.: On the mechanism of ion exchange in crystalline zirconium phosphates. I. Sodium ion exchange of α-zirconium phosphate. J. Phys. Chem. 73, 3424 (1969).
59. Cheng, Y., Zhang, H., Jaenicke, J. A., Tan, E. C. P., Chuah, G.-K.: Minimalistic Synthesis of α-Zirconium Diammonium Phosphate and Zirconia for Applications in Ion Exchange and Catalysis. ACS Sustainable Chemistry & Engineering 7, 895 (2019).
60. Casciola, M., Alberti, G., Donnadio, A., Pica, M., Marmottini, F., Bottino, A., Piaggio, P.: Gels of zirconium phosphate in organic solvents and their use for the preparation of polymeric nanocomposites. Journal of Materials Chemistry 15, 4262 (2005).
61. Sun, L., Boo, W. J., Sun, D., Clearfield, A., Sue, H.-J.: Preparation of Exfoliated Epoxy/α-Zirconium Phosphate Nanocomposites Containing High Aspect Ratio Nanoplatelets. Chemistry of Materials 19, 1749 (2007).
62. Sun, L., Boo, W. J., Sue, H.-J., Clearfield, A.: Preparation of α-zirconium phosphate nanoplatelets with wide variations in aspect ratios. New Journal of Chemistry 31, 39 (2007).
63. Trobajo, C., Khainakov, S. A., Espina, A., García, J. R.: On the synthesis of α-zirconium phosphate. Chem. Mater. 12, 1787 (2000).
64. Alberti, G., Torracca, E.: Crystalline insoluble salts of polybasic metals - II. Synthesis of crystalline zirconium or titanium phosphate by direct precipitation. J. Inorg. Nucl. Chem. 30, 317 (1968).
65. Cheng, Y., Wang, X., Jaenicke, S., Chuah, G.-K.: Minimalistic Liquid-Assisted Route to Highly Crystalline α-Zirconium Phosphate. ChemSusChem 10, 3235 (2017).
66. Harjula, R., in *Encyclopedia of Separation Science*, edited by I. D. Wilson, C. F. Poole, T. R. Adlard et al. (Academic Press, London, 2000), Vol. 2, pp. 1651.
67. Helfferich, F., *Ion Exchange*. (Dover, New York, 1995).
68. Patterson, A. L.: The Scherrer Formula for X-Ray Particle Size Determination. Physical Review 56, 978 (1939).
69. Muniz, F. T. L., Miranda, M. A. R., Morilla dos Santos, C., Sasaki, J. M.: The Scherrer equation and the dynamical theory of X-ray diffraction. Acta Crystallographica Section A 72, 385 (2016).
70. Holland, T. J. B., Redfern, S. A. T.: Unit cell refinement from powder diffraction data; the use of regression diagnostics. Mineralogical Magazine 61, 65 (1997).
71. Clayden, N. J.: Solid-state nuclear magnetic resonance spectroscopic study of [gamma]-zirconium phosphate. Journal of the Chemical Society, Dalton Transactions 1877 (1987).
72. MacLachlan, D. J., Morgan, K. R.: Phosphorus-31 solid-state NMR studies of the structure of amine-intercalated .alpha.-zirconium phosphate: reaction of .alpha.-zirconium phosphate with excess amine. The Journal of Physical Chemistry 94, 7656 (1990).
73. Casciola, M., Capitani, D., Comite, A., Donnadio, A., Frittella, V., Pica, M., Sganappa, M., Varzi, A.: Nafion–Zirconium Phosphate Nanocomposite Membranes with High Filler Loadings: Conductivity and Mechanical Properties. Fuel Cells 8, 217 (2008).
74. Casciola, M., Capitani, D., Donnadio, A., Frittella, V., Pica, M., Sganappa, M.: Preparation, Proton Conductivity and Mechanical Properties of Nafion 117–Zirconium Phosphate Sulphophenylphosphonate Composite Membranes. Fuel Cells 9, 381 (2009).
75. Pica, M., Donnadio, A., Capitani, D., Vivani, R., Troni, E., Casciola, M.: Advances in the Chemistry of Nanosized Zirconium Phosphates: A New Mild and Quick Route to the Synthesis of Nanocrystals. Inorganic Chemistry 50, 11623 (2011).